本完整報告，以由此計畫支持而完成之三篇論文為主。

1. Liu, T.-A., Liu, M.-C. and *Yang, Y.-S. (2008) Immunohistochemical Analysis of a Novel Dehydroepiandrosterone Sulfotransferase-like Protein in *Drosophila* Neural Circuits, *Biochem. Biophys. Res. Comm*., **367**, 14-20. (SCI)
2. Lu, L.-Y., Hsieh, Y.-C., Liu, M.-Y., Lin, Y.-H., Chen, C.-J. and *Yang, Y.-S. (2008) Identification and Characterization of Two Amino Acids Critical for the Substrate Inhibition of Human Dehydroepiandrosterone Sulfotransferase (SULT2A1) *Molecular Pharmacology*, **73**, 660-668. (SCI)
3. Huang, C.-Y., Hsu, C.-C., Chen, M.-C. and *Yang, Y.-S. (2008) Effect of metal binding and posttranslational lysine carboxylation on the activity of recombinant hydantoinase, *J. Bio Inorg Chem,* accepted. (SCI)

醯胺水解酵素超家族，包括醯亞胺水解酵素、尿囊素水解酵素、二氫乳清酸水解酵素、海因水解酵素…等，這類酵素雖然在一級序列比對上的相似度可能只有不到百分之三十，但都保留相同催化部份的結構。其中，被認為與酵素催化有非常重要的關聯並高度保留的有四個組胺酸、一個天門冬胺酸、以及一個經過後修飾的離胺酸與金屬離子螯合。此外，由序列與結構的比對也發現亞硫酸基轉移酵素與核苷酸激酶雖然序列相似度在百分之二十以下，但結構上卻有一定程度的相似，其特定結構的保留可能與特殊的受質/配體結合有關。此二類酵素之關連性的研究亦十分值得進一步研究。本計劃的目的在於整合生物資訊、生物化學以及分子生物學三種不同的途徑來更進一步了解這些酵素催化反應中的反應機制與功能相關性。另一方面，我們也計畫對此酵素之催化相關後修飾胺基酸以點突變方式進行解析。並嘗試解析這些胺基酸殘基對催化機制的影響。此外，針對亞硫酸基轉移酵素的部分，我們也利用本計畫發展的工具進行分析，並進行不同類別之酵素的單元融合進而創造出雙功能的人工酵素。
關鍵字：醯胺水解酵素超家族、醯亞胺水解酵素、亞硫酸基轉移酵素、核苷酸激酶。

Amidohydrolase superfamily includes imidase, allantoinase, dihydroorotase, hydantoinase, and other related enzymes that were proposed based on the rigidly conserved structural domains in identical positions. Although the overall sequence homology within the enzyme superfamily can be lower than 30%, these conserved regions, compose of four histidines, one aspartate, and one modified lysine which is bridging one or two metal ions are involved in the catalysis. In addition, sulfotransferases and nucleotide kinases were also found to be similar in structure but different in sequence identity (<20%). The conservation of structural features may be correlated to specific functions such as substrate/ligand binding. The goal of this proposal is to understand the mechanism and functional properties of these enzyme families by using combined techniques of bioinformatics, biochemistry and molecular biology. In particular, we would like to distinguish the need for either a binuclear or mononuclear metal centre in imide hydrolysis. During the past year, we use site-directed mutagenesis to evaluate the role of the catalytic residues predicted by FAVA. In addition, we mutate residue of the oligomerization interface of sulfotransferase and successfully created a chimerical bi-functional sulfotransferase.
Keywords: Amidohydrolase Superfamily, Imidase, Sulfotransferase, Nucleotide Kinase.

Immunohistochemical Analysis of a Novel Dehydroepiandrosterone Sulfotransferase-like Protein in *Drosophila* Neural Circuits

Tzu-An Liu[1], Ming-Cheh Liu[2] and Yuh-Shyong Yang[1,3*]

[1] Department of Biological Science and Technology and Institute of Biochemical Engineering, National Chiao Tung University, Hsinchu, Taiwan
[2] Department of Pharmacology, College of Pharmacy, The University of Toledo, Toledo, OH 43606 USA
[3] Instrument Technology Research Center and National Nano Device Laboratories, NARL, Hsinchu, Taiwan

*Corresponding author:
Dr. Yuh-Shyong Yang
Department of Biological Science and Technology,
National Chiao Tung University,
75 Po-Ai Street,
Hsinchu30050, TAIWAN
Fax: 886-3-5729288
E-mail: ysyang@faculty.nctu.edu.tw

ABSTRACT

Sulfotransferase (ST)-catalyzed sulfation plays an important role in various neuronal functions such as homeostasis of catecholamine neurotransmitters and hormones. *Drosophila* is a popular model for the study of memory and behavioral manifestations because it is able to mimic the intricate neuroregulation and recognition in humans. However, there has been no evidence indicating that cytosolic ST(s) is(are) present in *Drosophila*. The aim of this study is to investigate whether or not cytosolic ST(s) is(are) expressed in the *Drosophila* nervous system. Immunoblot analysis demonstrated the presence of dehydroepiandrosterone (DHEA) ST-like protein in *Drosophila* brain and a sensitive fluorometric assay revealed its sulfating activity toward DHEA. Immunohistochemical staining demonstrated this DHEA ST-like protein to be abundant in specific neurons as well as in several bundles of nerve fibers in *Drosophila*. Clarification of a possible link between ST and a neurotransmitter-mediated effect may eventually aid in designing approaches for alleviating neuronal disorders in humans.

Key words: sulfation; *Drosophila*; DHEA ST; memory; neuropharmacology

INTRODUCTION

Cytosolic STs are enzymes that catalyze the transfer of a sulfuryl group from the universal sulfate donor 3'-phophoadenosine 5'-phophosulfate (PAPS) to a variety of endogenous and exogenous compounds, such as steroids, amines, and various xenobiotic chemicals (1). The reaction, usually referred to as "sulfation", occurs in many prokaryotic and vertebrate species and plays an important role in numerous biological processes including hormone regulation, homeostasis of neurotransmitters, as well as transport and metabolism of steroids in circulation. The sulfation of steroids decreases their biological activity, rendering them incapable of binding and activating steroid receptors. These sulfated steroids, nevertheless, may serve as prohormones, which can be reactivated by desulfation (2). Although most steroids are synthesized in steriodogenic organs, a few, such as progesterone (PROG), pregnenolone (PREG) and DHEA, are produced *de novo* in the central nervous system (CNS) and peripheral nervous system (PNS) (3). These neurosteroids regulate specific gene expression and protein synthesis, cellular development, neuroendocrine functioning, and behavioral pattern (4). Dehydroepiandrosterone sulfotransferase (DHEA ST) catalyzes the sulfation of DHEA, converting it to dehydroepiandrosterone sulfate (DHEAS) (5). Both DHEA and DHEAS are critical precursors for the production of several types of androgens and estrogens. DHEA can also be metabolized to form testosterone, estradiol and androstenediol (6). DHEA and DHEAS are involved in numerous neurophysiological processes, such as increasing neuronal excitability, and enhancing neural plasticity and neuroprotective properties. Previous studies have demonstrated that the concentrations of DHEA and DHEAS in blood decrease markedly with age in humans, and have been proposed to be the neuromodulators involved in age-related cognitive decline (7). These findings have led to the hypothesis that elevated concentrations of steroids may influence both physical and cognitive aging.

Drosophila melanogaster is a popular animal model for pathological and neuropharmacological research. At the molecular level, the nervous system of the *Drosophila* can mimic the intricate neuroregulation of the neuronal network in humans. In *Drosophila*, several types of carbohydrate STs have been cloned and characterized, and the physical functions and biological regulations modulated by the sulfate conjugates have been extensively investigated (8). The sulfation of hexuronate and glucosamine units, usually *N*-acetylgalactosamine (GlaNAc) or *N*-acetylglucosamine (GlcNAc), has been shown to be essential for development and embryogenesis, as well as differentiation and neuronal functions (9). The recent studies have demonstrated that sulfation is a critical regulator for developmental and neuronal functions in *Drosophila*, however, there has been no evidence indicating that cytosolic ST(s) is(are) present in this important animal model. In the present work, we used a specific DHEA ST antibody to determine the existence and distribution of DHEA ST-like protein in the nervous system of *Drosophila*. Moreover, we investigated and confirmed the presence of DHEA-sulfating activity of in *Drosophila* brain extracts by employing a continuous fluorometric assay.

MATERIALS AND METHODS

Preparation of recombinant STs

Recombinant human phenol-preferring phenol sulfotransferase (*h*P-PST), human catecholamine-preferring phenol sulfotransferase (*h*M-PST), and *h*DHEA ST were cloned into an expression vector, pGEX-2TK, respectively, and transformed into

Escherichia coli BL21 (DE3). These STs were expressed in the form of GST-fusion protein and purified by glutathione (GSH)-bound sepharose. The methods of expression and purification of these three STs were described previously (10). Recombinant rat phenol sulfotransferase (*r*PST) was cloned into expression vector pET3c and transformed into *E. coli* BL21 (DE3). Briefly, DEAE, hydroxyapatite, and size-exclusion chromatography were used to purify the *r*PST (11). Putative *Drosophila* cytosolic ST, *dm*CG5431, was found on the Flybase database (CG5431; http://flybase.bio.indiana.edu/). By using RT-PCR, a full length cDNA encoding *dm*CG5431 was cloned into pET-41b and transformed into *E. coli* BL21 (DE3). GST-fusion and His-tagged ST was expressed and purified by GSH-bound sepharose and Ni-chelating column. All purified STs were in homogeneous form and determined by SDS-PAGE.

Indirected enzyme-linked immunosorbent assay (IELISA)

Approximately 1 µg of the recombinant STs, *h*P-PST, *h*M-PST, *h*DHEA ST, *r*PST and *dm*CG5431 were coated on each well of an ELISA plate for screening using *h*DHEA ST antibody. Following washes with PBS, 50 µl of serially diluted solutions of *h*DHEA ST antibody were added to individual wells and incubated for 1 h. Afterwards, each well was washed three times with PBST (PBS containing 0.1% BSA and 0.05% Tween-20). Bound antibodies were then detected using a goat anti-rabbit IgG conjugated with horseradish peroxidase (HRP) for 30 min in PBST. Finally, each well was washed and developed with 0.04% 2,2-azino-bis(3-ethylbenz-thiazoline-6-sulfonic acid) (ABTS) containing 0.01% H_2O_2 in PBS. For denatured conformation analysis, all steps were the same except that the recombinant STs were treated with 2% β-ME and heating prior to being coated on the wells.

Preparation of *Drosophila* brains homogenates

The *Drosophila* heads were freshly isolated by liquid nitrogen freezing and harvested through a sieve to separate the heads from the bodies. Approximately 0.2 g of frozen brain samples were homogenized using a mortar and pestle, dissolved in a lysis buffer (2 mM sucrose plus 3 mM β-ME, 0.2% Triton X-100 and 0.5% protease inhibitor cocktail in 10 mM HEPES buffer, pH 7.4) and then centrifuged to remove cell debris. The homogenate was centrifuged twice at 15,000 rpm for 20 min at 4°C. The supernatant was collected and the total protein concentration was estimated.

Immunoblot analysis

Approximately 5µg of five recombinant STs, *h*P-PST, *h*M-PST, *h*DHEA ST, *r*PST and *dm*CG5431, respectively, were loaded onto individual wells of a 12% SDS-PAGE for electrophoresis according to the method of Laemmli (12). After electrophoresis, the separated proteins were electroblotted onto a nitrocellulose membrane and blocked with 5% skimmed milk for 1 h. The membrane was incubated with *h*DHEA-ST antibody for 1 h and washed three times with PBST for 5 min. The membrane was then immersed in PBST containing antibody against rabbit IgG conjugated with HRP for 1 h. The bound antibodies were detected with an ECL western blotting reagents for chemiluminescent detection. The native immunoblot analysis procedure was similar to that described previously with minor modifications. All buffer solutions were free from the addition of SDS. Similarly, approximately 300 µg of *Drosophila* brain proteins and 20 µg of purified hDHEA ST were used for analyzing the protein expression of DHEA ST-like protein by native and SDS immunoblot. The steps were similar to those described previously.

Determination of sulfating activity of DHEA in *Drosophila* brain

DHEA-sulfating activity of *Drosophila* brain was determined by the continuous fluorometric assay developed by Chen et al. (13). By using DHEA as substrate, the

activity of DHEA ST was determined by monitoring the fluorescence intensity of MU. The standard assay mixture had a final volume of 1 ml, and contained 100 mM potassium phosphate buffer (pH 7.0), 5 mM β-ME, 20 μM PAPS, 4 mM MUS, 5 μM DHEA and 3.2 mU K65ER68G, the recombinant β-form of PST. For use in the assay, a partially purified DHEA ST-like protein fraction, located by cross-reactivity with antibody against *h*DHEA ST, was prepared from *Drosophila* brain homogenates by using native gel electrophoresis. The intensity of MU was monitored using a spectrofluorometer (Hitachi F-4500, Japan).

Immunohistochemistry

The *Drosophila* brain was perfused with 4% paraformaldehyde for fixation and then penetrated with 30% sucrose. After washing with PBS, the brain was blocked with 1% BSA overnight at 4°C to prevent nonspecific staining. The sample was then incubated with *h*DHEA ST antibody at 4°C for 72 h, rinsed with washing buffer (containing 0.1% BSA and 0.2% Triton X-100 in PBS, pH 7.4) for 20 min three times, and then stained with biotinylated goat anti-rabbit secondary antibody. After an overnight incubation at 4°C, the sample was washed with washing buffer for 20 min. Tertiary antibodies (streptavidin-Cy5 and biotinylated HRP) were also incubated with the brain sample overnight at 4°C. Afterwards, the brain sample was mounted using FocusClear™ and examined by confocal laser scanning microscope photomicrographs. The *Drosophila* carries gene trap Gal4 (12423) and UAS-GFP to expresses GFP in the DPM neurons (green) was used to analyze the colocalization of DHEA-ST like protein and DPM neuron. Steps were same as mentioned above (14).

RESULTS

Characterization of *h*DHEA ST antibody

The characterization of *h*DHEA ST antibody analyzed by IELISA and immunoblotting is shown in Fig. 1. The *h*DHEA ST antibody showed stronger affinity toward recombinant *h*DHEA ST and *dm*CG5431 in native conformations than the others co-tested (Fig. 1A). The dose-response curves showed that the *h*DHEA ST antibody was specific to *h*DHEA ST when the STs tested were first denatured by treating with β-ME and heating (Fig. 1B). The binding of *h*DHEA ST antibody to PST isoforms was barely discernible. The specificity of antibody for *h*DHEA ST was determined by probing five different types of recombinant STs by immunoblotting (Fig. 1C). The *h*DHEA ST antibody interacted with both *h*DHEA ST and *dm*CG5431 in their native forms, whereas neither *h*PST isoforms nor *r*PST was recognized. Furthermore, only *h*DHEA ST was identified by this specific antibody under the denatured conditions (Fig. 1D).

Expression of DHEA ST-like Protein in *Drosophila* brains

As shown in Fig. 2, the immunoblot of *Drosophila* brain extracts was analyzed by *h*DHEA ST antibody. The DHEA ST-like protein expressed in soluble extracts of *Drosophila* brains was recognized in its native form (Fig. 2A). The SDS-PAGE immunoblot showed that only *h*DHEA ST (positive control) was recognized when the native conformation was disrupted (Fig. 2B).

Localization of DHEA ST-like Protein in *Drosophila* brains

The distribution and relative abundance of DHEA ST-like protein in *Drosophila* brain are shown in Fig. 3. A total of six DHEA ST-like protein positive neurons were observed in the posterior section of *Drosophila* brain (Fig. 3A). Two DHEA ST-like protein positive neurons were also detected in the dorsal part of the brain (Fig. 3B). DHEA ST-like protein positive neuronal fibers, exhibiting the typical appearance of beaded nerve fibers, were seen throughout the entire *Drosophila* brain (Fig. 3C). Table

1 summarizes the relative localization and abundance of DHEA ST-like protein positive neurons and fibers. By using UAS-WGA as a trans-synaptic transmission marker and VAM-Gal4 as a driver, the colocalization of DHEA ST-like protein positive regions and DPM neuron were observed by transgenic fly that carries VAM-Gal4 and UAS-WGA and express WGA in the VAM neurons (Fig. 4).

Determination of the DHEA-sulfating activity in *Drosophila* brains

The sulfating activity of DHEA in partially purified *Drosophila* brain extract was assessed using a continuous fluormetric assay (Table 2). The complete system (I) could detect not only sulfating but also desulfating activities due to the presence of MUS. The DHEA-sulfating activity could not be observed in the absence of PAPS, and therefore reaction condition II gave a background activity exhibited mainly by arylsulfatase. As a result, the specific activity and total activity of DHEA-sulfating activities in *Drosophila* brain were determined to be 57.7 ± 12.1 pmole/min/mg and 0.7 ± 0.2 nmole/min/g, respectively. It is to be noted hat a high level of arylsulfatase activity (specific activity and total activity, 319.1 ± 7.5 pmol/min/mg and 6.8 ± 0.1 nmol/min/g, respectively) in the fraction was detected as well.

Discussion

To date twenty-three structures of cytosolic STs have been solved on eleven different isoforms. Crystal structures for the ST1A1 (phenol ST), ST1A3 (catecholamine ST), ST1E1 (estrogen ST), ST1B1 (thyronine ST), ST2A1 (DHEA ST), two isoenzymes of ST2B1 (pregnenolone ST and cholesterol ST), ST4A1 (neuronal ST) and three subfamilies of ST1C have been characterized. Structure-based sequence alignments indicate that the PAPS binding site, and structural fold, is highly conversed, albeit the homology of the amino acid sequences between different ST isoforms is not high (15). On the basis of the characteristic pattern of the STs, we demonstrated the possible presence of a cytosolic ST-like protein in *Drosophila* neural circuits by the specific recognition of the *h*DHEA ST antibody. The results obtained from immunoblot analysis and IELISA are close agreement with conserved nature of STs and indicate that STs may exert similar biological functions in various animals.

Drosophila is an excellent experimental model to systematically study the neuroregulative mechanisms in human CNS. Many scientists have placed much effort into the molecular characterization and physical relevance of STs in this tiny creature, however, the biological significance of STs in *Drosophila* remains obscure. In general, sulfate conjugation is apparently involved in the metabolism of juvenile hormones and ecdysteroids in insects (16). In *Prodenia eridania*, sulfate conjugation of ecdysteroids seems to play a critical role in embryonic development and puparium formation (17). In the present study, the protein partially purified from *Drosophila* brain extracts was demonstrated to be capable of transferring a sulfuryl group from a sulfate donor, PAPS, to an analog of ecdysteroid, DHEA, and the result was consistent with that reported for *Mosquito*, *Aedes togoi* (18) suggested that sulfation in various insect species may exhibit similar biological functions in the metabolism of free hormones and post-stage embryogenesis. Earlier studies had also revealed the existence of cytosolic STs in flies of *Diptera*, *Prodenia eridania* (19). In addition to its activity on *p*-nitrophenol, the ST prepared from *Prodenia eridania* gut was significantly active in the sulfation of the steroids, such as DHEA, oestrone, and insect moulting hormones α-ecdysone and 22,25-bisdeoxyecdysone. It appears logical to suggest that STs comprehensively regulate the biochemical transformations for the purpose of detoxication, others may have important physiological implications in insects. Besides,

it is noted that DHEA-sulfating activity in *Drosophila* was significantly lower than that in rat and human (20, 21). This is to be expected because DHEA is a more common substrate for DHEA ST in mammalians than in insects. Furthermore, the validity of such comparison is always open to some question in consideration of differences in enzyme preparation and enzymatic assay. Nevertheless, It is noteworthy that the significant level of arylsulfatase activity was determined (Table 2). In agreement with these previous findings, the low or undetectable DHEA ST activities may be due to high levels of steroid sulfatase in soluble extracts, thereby interfering with the determination of DHEA ST *in vitro* (22).

Several neural regions of *Drosophila* brain were found to have DHEA ST-like immunoreactivity in this study. The immunoreactivity was selectively localized in the neurons of posterior and dorsal part of *Drosophila* brain, and nerve fibers indicating the relevant molecular and neuronal mechanism between this enzyme and its metabolites. In *Drosophila*, there are several types of projection neuron that forward information out of the antennal lobes. Medial and outer antennocerebral tracts (mACT and oACT, respectively) protrude into the ill-defined region and the lateral horn, while the others carry information along the inner antennocerebral tracts (iACT) to the mushroom body (MB). In our study, we observed an abundance of *Drosophila* DHEA ST-like protein expressed in the lateral horn and iACT (Table 1). The results implied that the DHEA ST-like protein may act as a neuromodulator of the ecdysteroids, which are involved in memory formation in *Drosophila*. The finding is also consistent with the result reported by Johnson et al (23). The sulfate-conjugated steroid is essential to the process of memory retention and significantly enhanced the cognition and learning in rats. Basically, they act through γ-aminobutyric $acid_A$ ($GABA_A$) receptors, *N*-methyl-$_D$-aspartate (NMDA)-type glutamatergic receptors and sigma receptors to induce excitatory cellular actions or inhibit cellular properties.

Increasing evidences have suggested that DPM neuron may co-release *amnesiac* neuropeptide and acetylcholine in the *amnesiac* mutant flies (24). Transgenic expression of the *amnesiac* gene in the DPM neurons rescues the *amnesiac* memory phenotype, establishing a possible route between DPM neuron function and *amnesiac*-dependent memory. Additionally, the paired conditioning of unconditioned stimulus (US) (electric shock) and conditioned stimulus (CS) (odor stimulus) increases odor-evoked calcium signals and synaptic release from DPM neurons (25). These observations indicated that DPM neurons not only respond to the US pathway, but that they are also “odor generalists”, responding to all odors that were tested. The colocalization of DHEA ST-like protein and DPM neuron implied that DHEA ST-like protein may not merely play the role as a neuroregulator in the process of odor-specific memory trace in *Drosophila* but also involve in the modulation of specific memorial and behavioral formations.

ACKNOWLEDGMENT

This research was financially supported by National Science Foundation, under Grant NSC 96-96-2120-M-009-001 and 96-2627-B009-004. The authors deeply appreciate the technical contribution of Dr. Ann-Shyn Chiang, Institute of Biotechnology at National Tsing Hua University, and Ms. Pei-Chi Zheng, and Mr. Wei-Ti Chen, Institute of Biochemical Engineering at NCTU.

REFERENCES

[1] E. Chapman, M.D. Best, S.R. Hanson, C.H. Wong, Sulfotransferases: structure, mechanism, biological activity, inhibition and synthetic utility, Angew. Chem. Int. Ed.

43 (2004) 3526-3548.
[2] C.N. Falany, Enzymology of human cytosolic sulfotransferases, FESAB J. 11 (1997) 206-216.
[3] A.F. De Nicola, Steroid hormones and neuronal regeneration, Adv. Neurol. 59 (1993) 1199-1206.
[4] M. Vallée, W. Mayo, M.L. Maol, Role of pregnenolone, dehydroepiandrosterone and their sulfate esters on learning and memory in cognitive aging, Brain Res. Rev. 37 (2001) 301-312.
[5] C. Longcope, Dehydroepiandrosterone metabolism, J. Endocrinol. 150 (1996) S125-S127.
[6] J. Young, B. Couzinet, K. Nauhoul, S. Brailly, P. Chanson, E.E. Baulieu, G. Schaison, Panhypopituitarism as a model to study the metabolism of dehydroepiandrosterone (DHEA) in humans, J. Clin. Endocrinol. Metab. 82 (1997) 2578-2585.
[7] S. Legrain, L. Girard, Pharmacology and therapeutic effects of dehydroepiandrosterone in older subjects, Drugs Aging 20 (2003) 949-967.
[8] M. Kushe-Gullberg, L. Kjellén, Sulfotransferases in glycosaminoglycan biosynthesis, Curr. Opin. Struct. Biol. 13 (2003) 605-611.
[9] A.D. Lander, C.S. Stipp, J.K. Ivins, The glypican family of heparan sulfate proteoglycans: major cell-surface proteoglycans of the developing nervous system. Perspect. Dev. Neurobiol. 3 (1996) 347-358.
[10] Y. Sakakibara, Y. Takami, T. Nakayama, M. Suiko, M.C. Liu, Localization and functional analysis of the substrate specificity/catalytic domains of human M-form and P-form phenol sulfotransferases, J. Biol. Chem. 273 (1998) 6242-6247.
[11] T.M. Su, Y.S. Yang, Mechanism of posttranslational regulation of phenol sulfotransferase: expression of two enzyme forms through redox modification and nucleotide binding, Biochemistry 42 (2003) 6863-6870.
[12] U.K. Laemmli, Cleavage of structural proteins during the assembly of the head of bacteriophage T_4, Nature 227 (1970) 680-685.
[13] W.T. Chen, M.C. Liu, Y.S. Yang, Fluorometric assay for alcohol sulfotransferase, Ana. Biochem. 339 (2005) 54-60.
[14] Y. Wang, A.S. Chiang, S. Xia, T. Kitamoto, T. Tully, Y. Zhong, Blockade of neurotransmission in *Drosophila* mushroom bodies impairs odor attraction, Curr. Biol. 13 (2003) 1900-1904.
[15] V.L. Rath, D. Verdugo, S. Hemmerich, Sulfotransferase structural biology and inhibitor discovery, Drug Discov. Today 9 (2004) 1003-1011.
[16] A. Sannasi, P. Karlson, Metabolism of ecdysone: phosphate and sulphate esters as conjugates of ecdysone in *Calliphora vicina*, Zool. Jb. Physiol. 78 (1974) 378-386.
[17] M. Slade, C.F. Wilkinson, Degradation and conjugation of Cecropia juvenile hormone by the southern armyworm (*Predenia eridania*), Comp. Biochem. Physiol. 49 (1974) 99-103.
[18] L. Shampengtong, K.P. Wong, An in vitro assay of 20-hydroxyecdysone sulfotransferase in the mosquito, *Aedes togoi*, Insect Biochem. 19 (1989) 191-196.
[19] R.S. Yang, C.F. Wilkinson, Enzymatic sulphation of *p*-nitrophenol and steroids by larval gut tissues of the southern armyworm (*Prodenia eridania* cramer), Biochem. J. 130 (1972) 487-493.
[20] S. Aldred, R.H. Waring, Localization of dehydroepiandrosterone sulphotransferase in adult rat brain, Brain Res. Bull. 48 (1998) 291-296.
[21] T. Sugahara, Y.S. Yang, C.C. Liu, T.G. Pai, M.C. Liu, Sulphonation of dehydroepiandrosterone and neurosteroids: molecular cloning, expression, and

functional characterization of a novel zebrafish SULT2 cytosolic sulphotransferase, Biochem. J. 375 (2003) 785-791.
[22] G. Janer, S. Mesia-Vela, F.C. Kauffman, C. Porte, Sulfatase activity in the oyster *Crassostrea virginica*: its potential interference with sulfotransferase determination, Aquat. Toxicol. 74 (2005) 92-95.
[23] D.A. Johnson, T.H. Wu, P.K. Li, T.J. Mather, The effect of steroid sulfatase inhibition on learning and spatial memory, Brain Res. 865 (2000) 286-290.
[24] A.C. Keene, M. Stratmann, A. Keller, P.N. Perrat, L.B. Vosshall, S. Waddell, Diverse odor-conditioned memories require uniquely times dorsal paired medial neuron output, Neuron 44 (2004) 521-533.
[25] D. Yu, A.C. Keene, A. Srivatsan, S. Waddell, R.L. Davis, *Drosophila* DPM neurons forma delayed and branch-specific memory trance after olfactory classical conditioning, Cell 123 (2005) 945-957.

LEGENDS FOR FIGURE AND TABLE

Figure 1 The characterization of *h*DHEA ST antibody using recombinant STs and putative cytosolic ST of *Drosophila*. (A) The *h*DHEA ST antibody titre determined by IELISA using recombinant proteins in native conformation. (B) The *h*DHEA ST antibody titre determined by IELISA using recombinant proteins denatured by treatment with β-ME and heating. (C) Native immunoblot of the five recombinant proteins with *h*DHEA ST antibody. (D) SDS-PAGE immunoblot of the five recombinant proteins with *h*DHEA ST antibody. Each lane contained approximately 5 μg purified proteins.

Figure 2 The expression of DHEA ST-like protein in *Drosophila* brain extracts. (A) The native immunoblot of *Drosophila* brain extracts with *h*DHEA ST antibody. (B) SDS-PAGE immunoblot of *Drosophila* brain extracts and purified *h*DHEA ST with *h*DHEA ST. *dm*BE represented *Drosophila* brain extracts.

Figure 3 Distribution of the DHEA ST-like protein in *Drosophila* brain as illustrated by confocal laser scanning microscope. (A) DHEA ST-like protein selectively expressed in posterior region of brain. (B) DHEA ST-like protein expressed in dorsal part of the brain. (C) Expression of DHEA ST-like protein in neural fibers throughout the entire *Drosophila* brain. Granular staining suggests fibers labeled. 200X magnification.

Figure 4 Colocalization of the DHEA ST-like protein expression and DPM neuron in *Drosophila* brain. The arrowhead indicates the colocalization (orange) of DHEA ST-like protein (red) and DPM neuron (green) (400X magnification). *Right-lower*: the magnification of the colocalized region of DHEA ST-like protein and DPM neuron.

Table 1 Distribution and cellular colocalization of DHEA ST-like protein in *Drosophila* brain[a]

Brain region	Specific areas[b]	Neural cytoplasm[c]	Fibers[c]
Anterior brain			
	MB's vertical lobe	−	−
	superior medial PR	−	−
	median bundle	−	−
	MB satellite neuropil	−	−
	anterior optic tubercle	−	+
	ventrolateral PR	−	+
	MB's medial lobe	−	−
	antennal lobe	−	−
	antennal nerve	−	−
	ventral body	−	−
Middle brain			
	pedunculus	−	+
	fan-shaped body	−	+
	superior lateral PR	−	++
	ventral body	−	++
	superior medial PR	−	+
	tritocerebrum	−	++
	superior arch	−	+
	antennoglomerular tract	−	++
	ellipsoid body	−	+
	nodulus	−	++
	inferior lateral deutocerebrum	−	+
	Lo	−	++
	Medulla	−	+
Posterior brain			
	Lo	−	−
	LoP	−	++
	MB calyx	−	−
	PR bridge	+++	+
	ocellar nerve bundle	−	−

inner antennocerebral tract	−	+
lateral horn	+++	−
posterior lateral fascicle	−	++
SOG	−	+
axons of vertical cells of the LoP	−	++
axons of horizontal cells of the LoP	−	+
SOG nerves	−	−

[a]The distribution of DHEA ST-like protein in *Drosophila* brain was investigated by the continuous sections of the confocal laser scanning microscope photomicrographs. Detailed procedures were mentioned under *Materials and Methods* (14).

[b]Abbreviations: MB, mushroom body; PR, protocerebrum; Lo, lobula; LoP, lobula plate; SOG, subesophaeal ganglis; SOG nerves, roots of nerves from the fused subesophageal ganliea.

[c]The relative intensity of labeling was ranked by two independent observers. Ratings reflect mainly the density of DHEA ST-like protein labeled cell and fibers. Negative, −; weak, +; moderate, ++; strong +++.

Table 2 Sulfation and sulfatase activity in *Drosophila* brain[a]

		Fraction	
Reaction conditions	Enzyme activity involved	Specific activity (pmole/min/mg)	Total activity (nmole/min/g)
I. Complete[b]	DHEA-sulfating protein + arylsulfatase	376.8 ± 9.5	7.5 ± 0.2
II. – PAPS[c]	arylsulfatase	319.1 ± 7.5	6.8 ± 0.1
I – II	DHEA-sulfating protein	57.7 ± 12.1	0.7 ± 0.2
III. –Lysates	K65ER68G	16.6 ± 1.7	

[a]For use in the assay, a partially purified fraction which cross-react with antibody against *h*DHEA ST, was isolated from *Drosophila* brain homogenates by using native gel electrophoresis.

[b]Detailed procedures were described under *Coupled-enzyme assay for alcohol sulfotransferase (AST)* in *Materials and Method* (13). Specific activity referred to MU produced following the addition of extract whose protein concentration was determined by absorption at A_{280}. Total activity referred to MU produced with one gram of *Drosophila* brain extracts.

[c]AST activity was eliminated in the absence of PAPS (13).

Identification and Characterization of Two Amino Acids Critical for the Substrate Inhibition of Human Dehydroepiandrosterone Sulfotransferase (SULT2A1)

Lu-Yi Lu, Yin-Cheng Hsieh, Ming-Yih Liu, Yih-Hung Lin, Chun-Jung Chen and Yuh-Shyong Yang

Department of Biological Science and Technology, National Chiao Tung University, Hsinchu, Taiwan, ROC

a) Running Title: Substrate inhibition of sulfotransferase

b) Corresponding author:

Dr. Yuh-Shyong Yang

Department of Biological Science and Technology, National Chiao Tung University, Hsinchu, Taiwan, ROC

75 Po-Ai Street, Hsinchu30050, TAIWAN, ROC

Tel: +886-3-573-1983

Fax: +886-3-57-29288

E-mail: ysyang@faculty.nctu.edu.tw

c) Numbering:

Number of text pages: 42

Number of Tables: 5

Number of Figures: 5

Number of references: 40

Number of words in the Abstract: 212

Number of words in the Introduction: 539

Number of words in the Discussion: 1728

d) Abbreviations: SULT, sulfotransferase; PAPS, 3′-phosphoadenosine 5′-phosphosulfate; PAP, 3′-phosphoadenosine 5′-phosphate; DHEA, dehydroepiandrosterone; ADT, androsterone; MUS, 4-methylumbelliferyl sulfate; MU, 4-methylumbelliferone; *p*NP, *p*-nitrophenol.

Abstract

Substrate inhibition is a characteristic feature of many cytosolic sulfotransferases. The differences between the complex structures of SULT2A1/DHEA and SULT2A1/PAP or SULT2A1/ADT (PDB codes are: 1J99, 1EFH, and 1OV4, respectively) have enabled us to elucidate the specific amino acids responsible for substrate inhibition. Based on the structural analyses, substitution of the smaller residue alanine for Tyr-238 (Y238A) significantly increases the K_i value for dehydroepiandrosterone (DHEA) and totally eliminates substrate inhibition for androsterone (ADT). In addition, Met-137 is proposed to regulate the binding orientations of DHEA and ADT in SULT2A1. Complete elimination or regeneration of substrate inhibition for SULT2A1 with DHEA or ADT as substrate, respectively, was demonstrated with the mutations of Met-137 on Y238A mutant. Analysis of the Met-137 mutants and Met-137/Tyr-238 double mutants uncovered the relationship between substrate binding orientations and inhibition in SULT2A1. Our data indicate that, in the substrate inhibition mode, Tyr-238 regulates the release of bound substrate, and Met-137 controls substrate binding orientation of DHEA and ADT in SULT2A1. The proposed substrate inhibition mechanism is further confirmed by the crystal structures of SULT2A1 mutants at Met-137. We propose that both substrate binding orientations exhibit substrate inhibition. In addition, a corresponding residue in other cytosolic sulfotransferases was shown to have a function similar to that of Tyr-238 in SULT2A1.

Introduction

Sulfation is a widespread biological reaction catalyzed by members of the sulfotransferase (SULT) supergene family. These enzymes catalyze the transfer of a sulfuryl group from 3'-phosphoadenosine 5'-phosphosulfate (PAPS), the universal sulfuryl group donor molecule, to a substrate acceptor group. Cytosolic sulfotransferases catalyze sulfation of small molecules such as drugs, steroid hormones, chemical carcinogens, bile acids, and neurotransmitters (Mulder and Jakoby, 1990; Falany and Roth, 1993; Weinshilboum and Otterness, 1994; Glatt, 1997). Human SULT2A1 (dehydroepiandrosterone sulfotransferase, DHEA-ST) catalyzes the sulfation of various steroids and their derivatives, including hydroxysteroids such as dehydroepiandrosterone (DHEA), androsterone (ADT), testosterone, estradiol, and many other endogenous steroids (Falany, 1997; Chen et al., 1996; Kakuta et al., 1998). Steroid sulfation has been recognized as an important process for maintaining steroid hormone levels during their metabolism. In humans, dehydroepiandrosterone sulfate (DHEAS) is the most prevalent steroid precursor, and is one of the major secretory products of both adult and fetal adrenals (Chang et al., 2004).

Substrate inhibition is a common characteristic of sulfotransferases (Sugiyama et al., 1984; Marcus et al., 1980; Raftogianis et al., 1999; Ganguly et al., 1995). The catalysis and inhibition of DHEA and ADT by SULT2A1 have been reported to regulate the homeostasis and metabolism of these compounds and to maintain steroid levels (Chang et al., 2004). Previous studies have suggested that the onset of substrate inhibition is the formation of ternary dead-end complex (Duffel and Jakoby, 1981; Zhang et al., 1998). Furthermore, other kinetic studies also indicate that the dead-end complexes of E/PAP-SO_3/RO-SO_3 and E/PAP/ROH can be formed through either sequential random or ordered Bi Bi kinetic mechanisms (Zhang et al., 1998; Varin and Ibrahim, 1992; Marshall et al., 2000). This indicates that the changes of PAP affinity to sulfotransferase, for example in the different redox states for rat SULT1A1 (Marshall et al., 1997; Marshall et al., 2000), can affect substrate inhibition and enzyme activity. Furthermore, the substrate inhibition in SULT1A1 has been studied from X-ray crystal structure and compared with that of SULT1A3 which shares 93% amino acid sequence identity. The presence of two *p*-nitrophenol (*p*NP) molecules in the crystal structure of SULT1A1 explained the cooperativity and inhibition at low and high substrate concentrations, respectively (Barnett et al., 2004; Gamage et al., 2003). The stoichiometry of estradiol binding with human SULT1E1 was shown to have two ligands with one enzyme homodimer. Two binding sites were proposed as the catalytic and allosteric sites, respectively (Zhang et al., 1998). In a separate study, the crystal structure of SULT2A1 shows the presence of two orientations of DHEA in SULT2A1 (Rehse et al., 2002). There are interesting similarity and difference between SULT1A1 and SULT2A1 regarding their substrate binding orientations. However, the substrate inhibition in SULT2A1 has not been studied in detail.

Structural alignments among the complex structures of SULT2A1/ADT, SULT2A1/DHEA, and SULT2A1/PAP (Chang et al., 2004; Rehse et al., 2002; Pedersen et al., 2000) reveal spatial variation of amino acids in different substrate and PAP binding states. We herein describe experimental considerations that lead us to propose two of the amino acids, Tyr-238 and Met-137, are residues responsible in regulating substrate inhibition. Finally, we give another experimental example to demonstrate that the corresponding Tyr-238 residues of other cytosolic sulfotransferases possess the similar function as that of SULT2A1.

Materials and Methods

Materials

PfuTurbo DNA polymerase was purchased from Stratagene, and MUS, MU, DHEA, ADT, PAP, PAPS, *p*-nitrophenol, dopamine, glutathione (reduced form), and dithiothreitol (DTT) were purchased from Sigma (St. Louis, MO). Potassium phosphate (dibasic) was obtained from J. T. Baker (U.S.A.). DEAE Sepharose fast flow, Glutathione S-transferase Sepharose fast flow and Sephacryl S-100 HR were obtained from Amersham Pharmacia Biotech Asia Pacific (Hong Kong). All other chemicals were obtained commercially at the highest purity possible.

Methods

Site-Directed Mutagenesis of the cDNA Encoding SULT2A1, SULT1A1, and SULT1A3

Site-directed mutagenesis was performed with *PfuTurbo* DNA polymerase using QuickChange (Stratagene, La Jolla, CA). All primers for mutagenesis were purchased from Mission Biotech Co., Ltd. (Taiwan). Wild-type SULT2A1, SULT1A1, and SULT1A3 cDNA incorporated in the pGEX-2TK expression vector were used as templates in conjunction with specific mutagenic primers. Mutated cDNA sequences were confirmed using an ABI Prism 377 DNA sequencer (Applied Biosystems, Foster City, CA) following the standard protocol.

Expression, Purification and Characterization of Wild-type and Mutants of SULT2A1, SULT1A1, and SULT1A3

The expression and purification of SULT2A1, SULT1A1, and SULT1A3 were described previously (Sakakibara et al., 1998). Molecular weight of wild type (homodimer) and V260E mutant (monomer) of SULT2A1 was estimated by gel filtration chromatography. A homogeneous protein was obtained as determined by SDS-polyacrylamide gel electrophoresis (Laemmli, 1970).

Enzyme Assay

The activities of wild-type and mutant SULT2A1 were determined according to the change of fluorescence based on a coupled-enzyme assay method (Chen et al., 2005). The fluorescence of MU at 460 nm was measured upon excitation at 355 nm. The reaction mixture with a final volume of 1 ml consisted of 100 mM potassium phosphate buffer at pH 7.0, 5 mM 2-mercaptoethanol, 20 μM PAPS, 2 mM MUS, 5.4 μg K65ER68G (Yang et al., 1996) of rat SULT1A1, SULT2A1 and 5 μM of DHEA or ADT at 37 °C. A linear response was obtained when 1.49 to 14.9 nM (0.1 to 1 μg) SULT2A1 was added in the standard assay condition. In the reaction condition, excess amount of K65ER68G of rat SULT1A1 was added to catalyze the regeneration of PAPS so that the production of PAP catalyzed by SULT2A1 could not accumulate (Chen et al., 2005). The reaction condition for SULT1A3 standard assay was similar to that for SULT2A1 assay except that the reaction mixture contained 1.5 to 7.3 nM (0.1 to 0.5 μg) SULT1A3 and 30 μM of dopamine at 37 °C to replace SULT2A1 and DHEA or ADT, respectively. The control experiments of the coupled-enzyme assay were performed in the absence of PAPS, dopamine, MUS, SULT1A3, and K65ER68G of rat SULT1A1, respectively. Only the complete reaction renders the fluorometric activity of SULT1A3. K65ER68G of rat SULT1A1 is inactive toward DHEA, ADT and dopamine in the conditions described above. Activity of SULT1A1 was determined according to the change of absorbency at 400 nm due to elimination of free *p*-nitrophenol (ε = 10500 $M^{-1}cm^{-1}$ at pH 7.0) as described previously (Yang et al., 1996). The reaction mixture consisted of 100 mM potassium phosphate buffer at pH 7.0, 1 to 100 nM (0.07 to 7 μg) SULT1A1, 50 μM PAPS, 5 mM 2-mercaptoethanol, and 5 μM *p*-nitrophenol at 37 °C.

Substrate Binding

The dissociation constants (K_d) of PAP, DHEA, ADT towards SULT2A1, respectively, were determined with a spectrofluorimeter as described previously (Zhang et al., 1998). The decrease in intrinsic fluorescence of protein at 340 nm was observed upon excitation at 280 nm when an aliquot amount of PAP was added into the mixture consisted of 100 mM potassium phosphate buffer at pH 7.0, 100 nM wild-type or mutant SULT2A1 and varying concentrations of PAP at 25 °C with a final volume of 1.3 ml in a quartz cuvette of 1 cm square cross-section. In the formation of ternary dead-end complex, DHEA and ADT were added into the pre-incubated solution containing 0.5 μM wild type or mutants of SULT2A1, 100 mM potassium phosphate at pH 7.0, and 1 μM PAP at 25 °C. Each data point was duplicated, and the difference was within 10%.

Analysis of Kinetic Data

Results of kinetic experiments were analyzed using nonlinear regression to fit the appropriate

equation to the data. Kinetic data obtained from non-inhibitory experiments were individually fit to Michaelis-Menten Equation 1, and substrate inhibition data were fitted to substrate inhibition Equation 2 (Cornish-Bowden, 1995). The rate constants (K_m, V_{max}, and K_i) were obtained using SigmaPlot 2001, V7.0 and Enzyme Kinetics Module, V1.1 (SPSS Inc., Chicago, IL). Data used represent mean values derived from two determinations.

$v = V[S]/(K_m + [S])$ (Eq. 1)

$v = V[S]/\{K_m + [S](1 + [S]/K_i)\}$ (Eq. 2)

Protein Crystallization and Data Collection

Crystallization of M137I and M137W mutants was performed by the hanging-drop vapor-diffusion method at 18 °C. This condition was further refined to produce larger crystals using 2 μL hanging drops containing equal volumes of protein solution (1 μL) and a reservoir solution (1 μL) containing $(NH_4)_2SO_4$ (1.6 M), NaCl (100 mM) and HEPES (0.1 M) at pH 7.5. The crystals of M137I and M137W appeared within 3 days and grew to maximum dimensions after 7 days.

Crystallographic Data Collection and Processing

The crystals of diffraction quality were mounted on a Cryo-loop (0.1-0.2 mm), dipped briefly in 20 % glycerol as a cryo-protectant solution, and frozen in liquid nitrogen. X-ray diffraction data were collected at 110 K using the synchrotron radiation on the beamline BL13B1 at NSRRC (Hsinchu, Taiwan). The data were indexed and processed using the *HKL2000* program (Otwinowski and Minor, 1997). Details of the data statistics are given in the Table 5.

Crystal Structure Determination and Refinement

The structures of the M137I and M137W were determined by molecular replacement as implemented in *CNS v1.1* (Brunger et al., 1998) using the crystal structure of human dehydroepiandrosterone sulfotansferase (PDB code 1OV4) (Chang et al., 2004) as a search model. The M137I and M137W molecule was located in the asymmetry unit after rotation and translation function searches. All refinement procedures were performed using *CNS v1.1*. The composite omitted electron density maps with coefficients $|2F_o - F_c|$ were calculated and visualized using *O v11.0.4* (Jones et al., 1991), and the model was rebuilt and adjusted iteratively as required. Throughout the refinement, a random selection (10 %) of the data was placed aside as a "free data set", and the model was refined against the rest of the data with $F \geq 0$ as a working set. The monomer protein model was initially refined by rigid-body refinement using the data from 30.0 to 3.0 Å-resolution, for which the group temperature B values were first restrained to 20 $Å^2$. This refinement was followed by simulated annealing using a slow cooling

protocol with a starting temperature 2500 K, provided in *CNS*, applied to all data between 20.0 and 2.6 Å and 3.0 Å, respectively, for M137I and M137W. The bulk solvent correction was then applied, and group *B* factors were adjusted. After several cycles of positional and grouped *B* factor refinement interspersed with interactive modeling, the *R*-factors for the M137I and M137W complex decreased. The refinement then proceeded with another cycle of simulated annealing with a slow cooling with a starting temperature of 1000 K.

Model Validation

The correctness of stereochemistry of the model was verified using *PROCHECK* (Laskowski et al., 1993). The calculations of r.m.s. deviations from ideality for bonds, angles, and dihedral and improper angles performed in *CNS* showed satisfactory stereochemistry. In a Ramachandran plot (Ramachandran and Sasisekharan, 1968), all of main chain dihedral angles were in the most favored and additionally allowed regions. The refinement statistics are given in the Table 5.

Coordinates

Atomic coordinates for the crystal structures of M137I and M137W mutants described in this work have been deposited in the PDB (access code 2QP3 and 2QP4, respectively).

Results

Predicting Critical Amino Acid Residues for Substrate Inhibition by the Comparison of the Structure of SULT2A1 Complexes—Comparison between the SULT2A1/DHEA and SULT2A1/PAP binary complex structures may reveal the alternative locations of the main regulatory amino acid residues when substrate is present or absent in the active site. The overall structure of the SULT2A1/PAP complex is very similar to that of the SULT2A1/DHEA complex, except for some residues and a loop from residues Tyr-231 to Gly-252 (Table 1). The root-mean-square deviation (RMSD) value of this loop between the two structures is 6.67 Å for the backbone (excluding Lys-242 and Thr-243, which were not resolved in the SULT2A1/PAP binary complex structure). As shown in Figure 1A, the main difference near the DHEA binding site between the two complexes is that the loop from residues Tyr-231 to Tyr-238 is closed in SULT2A1/PAP, while it is open in SULT2A1/DHEA (Rehse et al., 2002; Pedersen et al., 2000). Furthermore, in the SULT2A1/DHEA complex, several hydrophobic residues on this loop, including Tyr-231, Leu-234, and Tyr-238, are located in close proximity to the DHEA molecule; these residues contribute to the hydrophobic nature of the active site. Also, in the SULT2A1/DHEA binary complex structure, Tyr-238 acts likely as the gate toward the substrate-binding cavity, but moves away from the active site in the SULT2A1/PAP binary

complex structure (Figure 1A). It is therefore reasonable to speculate that Tyr-238 may play a critical role in regulating the release of substrate. As shown in Figure 1B, the ADT molecule shares the same location as that of the DHEA molecule in the previously proposed alternative orientation (Rehse et al., 2002). The SULT2A1/DHEA and SULT2A1/ADT complex structures are quite similar at this region, including the loop described above, and the location of Tyr-238 residue.

Kinetic Analysis of Tyr-238 Mutants of SULT2A1— The hypothesized gate residue of Tyr-238 for regulating substrate inhibition, as revealed by the above structural comparison, was confirmed by site-directed mutagenesis. V_{max}, K_m and K_i values of wild type and Tyr-238 mutants (Y238A, Y238F, and Y238W of SULT2A1) were determined using DHEA or ADT as substrates (Table 2). Y238A of SULT2A1 exhibited no substrate inhibition when ADT was used as substrate and the K_i value of DHEA increased 7.4 folds as compared to that of wild type SULT2A1. The K_i values of DHEA and ADT for Y238F and Y238W of SULT2A1 also increased for about 2 to 3 folds as compared to those of wild type. The changes of K_m and V_{max} for Y238A, Y238F and Y238W ranged only from approximately 0.3 to 1.3 folds whenever DHEA or ADT was used as substrate (Table 2). This observation, consistent with the above prediction base on structural analysis, showed that Tyr-238 is regulating the substrate inhibition and demonstrated that the size of this amino acid side chain is important.

Predicting Amino Acid Residue Delineates the Orientations of DHEA and ADT in SULT2A1—Mutating Tyr-238 to alanine completely and partially eliminate the substrate inhibition for ADT and DHEA, respectively (Table 2), indicating that the additional amino acid(s) may be interacting with these two substrates in a different way since a single mutation (Tyr-238) is not capable of completely eliminating inhibition of both substrates. The complex structures of SULT2A1/DHEA and SULT2A1/ADT revealed two orientations for DHEA but only one for ADT as described earlier (Chang et al., 2004). Based on the available information, we might infer that the additional amino acid(s) that affect the substrate inhibition of DHEA may also affect its binding orientation in SULT2A1. To search for the possible amino acid(s), we superimposed the structures of SULT2A1/DHEA and SULT2A1/ADT on each other. Most of the amino acid residues hold the same positions in two complex structures, except for the side chains of Met-16, Ile-71, and Met-137 whose RMSD values (2.41, 2.50, and 2.40 Å, respectively) are noticeably higher than those of the others (Figure 2). Both Met-16 and Ile-71 of the SULT2A1/DHEA and SULT2A1/ADT complex structures form similar van der Waals interactions toward ADT and DHEA in the two orientations. By contrast, the C_ε atom of the Met-137 residue in SULT2A1/ADT complex structure points inward the substrate binding site and causes steric hindrance for ADT and prevents it from forming additional orientation observed only for DHEA. The shortest distance would have been only 1.11 Å between C-12 of

DHEA at this additional orientation and the C_ε atom of Met-137 in SULT2A1/ADT complex (Figure 2). From the structural analysis between SULT2A1/DHEA and SULT2A1/ADT complexes, it is reasonable to propose that, in addition to Tyr-238, Met 137 may serve as the amino acid that modulates the substrate inhibition and binding orientations of DHEA and ADT.

Kinetic Analysis of Met-137 and Met-137/Tyr-238 Mutants of SULT2A1—The proposed effects of Met-137 on substrate inhibition were examined by mutational analysis of SULT2A1 at Met-137 and Tyr-238. When Met-137 of SULT2A1 was mutated to isoleucine (M137I) and valine (M137V) which contain smaller side chains, K_i values for ADT increase over one order of magnitude (28.6 folds for M137I and 11.1 folds for M137V) (Table 2). The K_i value increases only 5.4 folds when Met-137 was mutated to larger side chain, tryptophan (M137W). Changes of K_i values for DHEA were in a similar trend to those of ADT with smaller increases (5.9, 8.7, and 1.2 folds for M137I, M137V, and M137W, respectively) (Table 2). M137K was also prepared and exhibited no enzymatic activity, most probably due to the positive charge of lysine that interferes with the hydrophobicity of the binding site.

These observations are consistent with the above structural analysis that Met-137 side chain is a steric hindrance for ADT in SULT2A1/ADT complex but not for DHEA in SULT2A1/DHEA complex (Figure 2). By removing this steric hindrance, additional binding orientation for ADT may form and result in considerable changes (over one order of magnitude) of their K_i values (M137I and M137V in Table 2). This proposal also agrees with our finding that the orientation of ADT may be disturbed when Met-137 is replaced with a smaller isoleucine (M137I/Y238A in Table 2) so that the substrate inhibition of ADT with M137I/Y238A can be observed. In contrast, by replacing a large side chain at Met-137 (M137W), additional steric hindrance may be created and one of the binding orientations of DHEA may be removed. This also predicts that, with additional mutation on Y238A at Met-137, the substrate inhibition for DHEA may be completely eliminated. Double mutations on SULT2A1 at Met-137 and Tyr-238 confirm our hypothesis (M137W/Y238A in Table 2). Two other double mutants, M137V/Y238A and M137K/Y238A (Table 2), also exhibited expected properties. The K_i values obtained with M137V/Y238A were between those obtained with M137I/Y238A and M137W/Y238A. M137K/Y238A still exhibited no enzymatic activity as that of M137K.

Comparison of the Crystal Structure of Wild-type, M137I, and M137W of SULT2A1—The data discussed above indicate that the additional substrate binding orientation modulated by Met-137 may be responsible for the substrate inhibition observed in Y238A only for DHEA but not for ADT (Table 2). The crystal structures of M137I and M137W in this study were determined and showed that the each global structure was similar to that of the wild-type, either the SULT2A1/DHEA or SULT2A1/ADT complex structure. In Figure 3, the structures of the residue Met-137 in SULT2A1 were compared to those of isoleucine (M137I) and tryptophan

(M137W) in SULT2A1 mutants. Replacing Met-137 with tryptophan (M137W) obviously contributes to steric hindrance and prevents the formation of the additional orientation of DHEA. This structural information is consistent with our hypothesis that the additional orientation of DHEA is responsible for the substrate inhibition in Y238A. As shown in Table 2, the DHEA substrate inhibition in Y238A can be eliminated in M137W/Y238A. On the contrary, replacing Met-137 with isoleucine (M137I) may remove the steric hindrance and provides a space for the formation of additional orientation for ADT in SULT2A1 (Figure 3). As shown in Table 2, the ADT substrate inhibition of Y238A can be regenerated with M137I/Y238A. Combination of the structural and kinetic data strongly supports our hypothesis that both Tyr-238 and Met-137 of SULT2A1 are responsible for the regulation of substrate inhibition as described above.

Dissociation Constants of PAP, DHEA and ADT in Binary and Ternary Complex Structures of SULT2A1 and Its Mutants—It is important to show that this ternary complex is intact in SULT2A1 mutants (Y238A, M137I, M137W, M137I/Y238A and M137W/Y238A) to support our proposal that Met-137 and Tyr-238 directly modulate substrate inhibition. As shown in Table 3, the dissociation constants of PAP of SULT2A1/PAP binary complexes are the same among wild type and all the mutants. Tight binding of PAP (in nM range as shown in Table 3) to the SULT2A1 and its mutants indicates that PAP binding site remains intact following such mutations. This information excludes the possibility that the change of K_i values reported in this study is due to the change of PAP binding to SULT2A1 mutants.

Affinity of either DHEA or ADT to SULT2A1/PAP binary complex was noticeably decreased whenever there is an Y238A mutant (Y238A, M137I/Y238A, and M137W/Y238A) as compared to that with wild-type SULT2A1 (Table 3). Except for the DHEA with M137I, mutation at Met-137 (M137I or M137W) did not significantly affect the binding of either DHEA or ADT to the SULT2A1/PAP binary complex. The dissociation constants of ligands (PAP, DHEA and ADT) and the double mutants of SULT2A1, M137I/Y238A and M137W/Y238A, are very similar to those with single mutant, Y238A (Table 3). These observations are consistent with the proposed function of Tyr-238 and Met-137 that the former acts to prevent the release of bound substrate while the later modulates the orientations of bound substrate in the substrate inhibition mode.

Substrate Inhibition in SULT2A1 Monomer—To examine the previous hypothesis that dimerization results in substrate blocking, the monomer mutant (V260E) of SULT2A1, designated in the KTVE motif (Petrotchenko et al., 2001) along with a double mutant, Y238A/V260E (Table 2), were constructed to comprehend the substrate inhibition of SULT2A1. The wild-type SULT2A1 (homodimer) was found to have similar kinetic constants as those of the mutant monomer. Furthermore, the pattern of substrate inhibition in monomer mutant (V260E in Table 2) is the same as that of wild-type SULT2A1. The mutation of monomer

mutant at Tyr-238 (Y238A/V260E in Table 2) also gives exactly the same substrate inhibition pattern as that of Y238A of SULT2A1 (Table 2). Data obtained from this study indicates that dimer or monomer of SULT2A1 does not play an important role for the exhibition of substrate inhibition.

Functional Analysis of Tyr-238 and Met-137 Corresponding Residues in Other Sulfotransferases—The multiple sequence and structure alignments of some solved-structure sulfotransferases are shown in Figure 4. In upper left of Figure 4, the residues corresponding to Tyr-238 of SULT2A1 have been highlighted, and they are as follows: Phe-247 of human SULT1A1, Leu-247 of human SULT1A3, Met-247 of mouse SULT1E1, Leu-249 of human SULT2B1_v1 (Gamage et al., 2003; Lu et al., 2005; Kakuta et al., 1997; Lee et al., 2003). This comparison leads us to hypothesize that the Tyr-238 corresponding residue in other sulfotransferases may play a similar role in substrate inhibition because these residues all demonstrate possible steric hindrance for the release of substrate from the substrate-binding cavity, and therefore they may modulate substrate inhibition for their own preferred substrates. To characterize the function of the SULT2A1 Tyr-238 corresponding residues in other sulfotransferases, further mutational analysis was conducted with SULT1A1 and SULT1A3 at Phe-247 and Leu-247 residue, respectively (Table 4). As compared to those of wild type SULT1A1, the K_i value of F247A (with *p*-nitrophenol as substrate) increased approximately 12-fold, the V_{max}/K_m value increased approximately 3-fold, while K_m remains pretty much the same. The K_i value of dopamine for SULT1A3 is much higher than that of *p*NP for SULT1A1 (Table 4). The positively charged dopamine at the assay condition may contribute to this difference. Mutations at Leu-247 of SULT1A3 give K_i values comparable with the size of the side chain of the mutated amino acid (the larger the amino acid side chain, the lower the K_i value) as shown in Table 4 for L247A and L247Y. The data from these investigations support our hypotheses that substrate inhibition in SULT2A1 is modulated by Tyr-238, and that analogous residues of Tyr-238 in other cytosolic sulfotransferases play similar roles with respect to substrate inhibition.

Discussion

Recently, the study in structure and function of enzymes has been greatly facilitated as a result of an expansion by means of their X-ray crystal structures. Crystal structures of SULT2A1 containing ADT, DHEA, and PAP, respectively, have been previously reported (Chang et al., 2004; Rehse et al., 2002; Pedersen et al., 2000). DHEA has been found to have two binding orientations in SULT2A1 (Rehse et al., 2002), however, bound ADT possesses only one, in which it is flipped over along the long axis of the DHEA relative to the proposed alternative

orientation (Chang et al., 2004). The previously proposed alternative orientation of DHEA was speculated to be a substrate-inhibition orientation owing to the fact that it placed O-3 hydroxyl group of DHEA with respect to His-99 for 2.9 Å away, and closer to the modeled PAP. Furthermore, it contained more van der Waals interactions with hydrophobic residues than the proposed catalytic orientation (Rehse et al., 2002). Prior study (Gamage et al., 2005) however, suggested that this would not result in substrate inhibition because this would require a relative increase in the proportion of the proposed alternative orientation while the substrate concentration increases. It might infer that both the orientations of DHEA could cause substrate inhibition while PAP remained in the active site to form ternary dead-end complex. In this report, we identified two amino acids (Met-137 and Tyr-238) responsible for modulating substrate inhibition of DHEA and ADT and were able to provide experimental evidences to show that both substrate binding orientations indeed cause substrate inhibition.

The bound orientations observed for DHEA and ADT might be in the substrate inhibition mode because the crystals were usually formed under high concentration of ligands although PAP was not present in the solved crystal structures of SULT2A1/DHEA and SULT2A1/ADT (Chang et al., 2004; Rehse et al., 2002). Dissociation constants of DHEA for SULT2A1 and its mutants at Tyr-238 and Met-137 (Table 3) also indicate that substrate inhibition may be induced by two possible binding orientations for DHEA because the substrate inhibition could be eliminated only after two specific mutations (M137W/Y238A in Table 2). According to the crystal structures of SULT2A1 (Figure 1B), Tyr-238 has weak interactions with ADT and the closest distance between Tyr-238 and the substrates is about 4.6 Å. Structural analyses among SULT2A1 complexes (Figure 1A and 1B) strongly suggest that Tyr-238 acts as a gate residue to regulate the release of substrate from the substrate-binding cavity in a ternary dead-end complex. The dissociation constants of ternary dead-end complex shown in Table 3 also support this implication. K_d values of both DHEA and ADT increase significantly when Tyr-238 was mutated to alanine. However, mutation of Tyr-238 alone can not completely eliminate DHEA substrate inhibition (Y238A in Table 2) indicating the existence of an additional substrate inhibition mode for DHEA but not for ADT. Structural analysis showed that Met-137 is closely interacting with DHEA and ADT and may modulate the substrate binding orientation (Figure 2). This scheme agrees with the experimental data that further mutation on Y238A at Met-137 not only can completely eliminate substrate inhibition for DHEA (M137W/Y238A in Table 2) but can also create substrate inhibition for ADT (M137I/Y238A in Table 2). These data strongly suggest that DHEA exists in only one orientation in M137W/Y238A and ADT presents in two orientations in M137I/Y238A. Comparison of the solved crystal structures shown in Figure 3 gives additional support for the proposed substrate binding orientations in these mutants.

As shown in Figure 4, other cytosolic sulfotransferases may also provide space for

substrates with two binding orientations. It has been proposed that substrate inhibition in SULT1A1 by estradiol could occur from the mis-orientation of substrate in the complex (Gamage et al., 2005). The presence of two *p*NP molecules in the crystal structure of SULT1A1 was postulated to explain cooperativity at low and inhibition at high substrate concentrations, respectively (Barnett et al., 2004). For SULT2A1, the K_i values shown in Table 2 indicate that Met-137 and Tyr-238 may modulate substrate inhibition at low and high K_i values, respectively. For ADT, the K_i value is significantly increased when the additional substrate binding orientation is proposed to present in the enzyme (M137I and M137I/Y238A in Table 2). The binding of substrates to Y238A is significantly loosened with PAP and enzyme complex (Table 3). This may either totally eliminate substrate inhibition (for ADT) or significantly decrease the substrate inhibition contribution from the substrate bound at the additional orientation (for DHEA). This scheme is consistent with the K_i value described previously for the reduced form of rat SULT1A1 that K_i is proposed to be determined by the binding constant of substrate and PAP/enzyme binary complex (Marshall et al., 2000).

Other possible causes for substrate inhibition proposed previously (Petrotchenko et al., 2001) were also examined in this study. In a previous study on SULT2A1/PAP complex structure (Pedersen et al., 2000), the loop of residues 231-252 shown in Figure 1A was speculated to prevent substrate binding while being involved in the dimer interface. This implies that the dimer may be an inactive form, with the second subunit of the dimer contributing to the locking in the substrate-blocking loop. Dimerization of SULT2A1 is not important for the substrate inhibition for exactly the same substrate inhibition patterns were observed for enzyme monomer, dimer and their mutants (Table 2).

The cause of sulfotransferase substrate inhibition has been attributed to the formation of an enzyme, substrate and PAP ternary complex (Duffel and Jakoby, 1981; Zhang et al., 1998). The binding of PAP is critical for the formation of the ternary complex (Hsiao and Yang, 2002) and it has been shown that affinity of PAP had profound effects on the activity of sulfotransferases (Marshall et al., 2000; Yang et al., 1996). Binding of PAP may significantly affect the substrate binding (Hsiao and Yang, 2002) and in turn affect substrate inhibition. This indicates that the changes of PAP affinity to sulfotransferase can affect substrate inhibition and enzyme activity. For example, rat SULT1A1 has been shown to significantly alter the transfer and physiological reactions in various redox states (Marshall et al., 1997). Mutation at other amino acid may also alter the PAP affinity to sulfotransferase (Hsiao and Yang, 2002; Yang et al., 1996). Mutation at Met-137 and Tyr-238 did not affect the nucleotide binding affinity to SULT2A1 (Table 3). In addition, the variations of the dissociation constants of DHEA and ADT in Tyr-238 and Met-137 mutants (Table 3) is consistent with what would be expected for the proposed functions of these two amino acids. Tyr-238 is proposed to modulate the release of bound substrate and can

significantly affect the dissociation constants of substrates when mutated.

In contrast, Met-137 is proposed to modulate the binding orientation of substrates and may not significantly change the dissociation constants of substrates when mutated. Comparison for Met-137 and its corresponding residues in other sulfotransferases is shown in lower middle of Figure 4. It is very interesting to observe that substrates used for various cytosolic sulfotransferase, shown on the upper right side of Figure 4, all align in either directions as those of DHEA in human SULT2A1 (Figure 2 and Figure 4). Human SULT1A1 contains two smaller substrates (*p*NP) that also locate in the two directions, respectively. Although Met-137 is postulated to function as modulator of substrate orientation in SULT2A1, it may not have the same function in other sulfotransferases. In fact, a nearby Val-148 instead of corresponding Ala-146 of human SULT1A1 is found to interact directly with *p*NP (Barnett et al., 2004). However, this comparison indicates that the two orientations of substrate binding in cytosolic sulfotransferases may be a common feature and it should be interesting to explore its functional meaning in enzyme catalysis.

The overall proposed model for the substrate binding orientation and inhibition modulated by Met-137 and Tyr-238 of SULT2A1 is depicted in Figure 5. Wild type SULT2A1 exhibits substrate inhibition by using either DHEA or ADT as substrates while the PAP is present. In the mutant Y238A, there is no substrate inhibition can be observed for ADT (with only one binding orientation) and less significant substrate inhibition for DHEA (with two binding orientations) than that of wild type SULT2A1. Mutation at Met-137 proposed to regulate the substrate binding orientation in this study can not completely eliminate substrate inhibition (M137I and M137W in Table 2) either the mutant contains space for two substrate binding orientations (M137I) or for only one substrate binding orientation (M137W). The relationship between the substrate binding orientations and substrate inhibition was uncovered when double mutations at Tyr-238 and Met-137 were examined. Although K_i values of both ADT and DHEA in mutant M137I/Y238A increase significantly as compared to those of M137I and wild type SULT2A1 (Table 2), substrate inhibition can not be completely removed because this mutant contains space for two binding orientations for both substrates. In contrast, M137W/Y238A exhibits no substrate inhibition by using either DHEA or ADT as substrate because this mutant can accommodate substrates in only one binding orientation.

Finally, the corresponding residues of SULT2A1 Tyr-238 in other cytosolic sulfotransferases are found to exhibit similar function in modulating substrate inhibition. Our study confirms that Phe-247 of SULT1A1, which corresponds to Tyr-238 of SULT2A1, is also important for substrate inhibition of *p*NP (Table 4). Previous researches on substrate inhibition of SULT1A1 (Barnett et al., 2004; Gamage et al., 2003) revealed that SULT1A1 could accommodate two *p*NP which leads to the substrate inhibition. Similarly, a higher or lower K_i

value of dopamine is obtained for SULT1A3 when Leu-247, the corresponding residue to SULT2A1 Tyr-238, is mutated to a smaller or larger amino acid, alanine or tyrosine, respectively (Table 4). It is also consistent with the above discussion that the substrate inhibition (*p*NP) of SULT1A1 can not be completely eliminated (Table 4) with a single mutation at the corresponding position of Tyr-238 of SULT2A1 (*i.e.* Phe-247) for two possible binding orientations (and two bound substrates) also exist for *p*NP in SULT2A1 (Figure 4). We therefore propose that the Tyr-238 and its corresponding residues in other cytosolic sulfotransferases play the similar role on regulating the release of substrate.

In conclusion, we propose that the substrate inhibition in SULT2A1 could occur from either orientation of substrate binding in the complex. The proposed function of Tyr-238 and Met-137 in SULT2A1 in this study may also be a model to explain how the substrate inhibition is modulated in other cytosolic sulfotransferases.

Acknowledgement

We thank Mr. Quillan Huang for proof reading the manuscript.

References

Barnett AC, Tsvetanov S, Gamage N, Martin JL, Duggleby RG and McManus ME (2004) Active site mutations and substrate inhibition in human sulfotransferase 1A1 and 1A3. *J Biol Chem* **279**:18799–18805.

Brunger AT, Adams PD, Clore GM, DeLano WL, Gros P, Grosse-Kunstleve RW, Jiang JS, Kuszewski J, Nilges M, Pannu NS, Read RJ, Rice LM, Simonson T and Warren GL (1998) Crystallography & NMR system: A new software suite for macromolecular structure determination. *Acta Crystallogr D* **54**:905–921.

Chang HJ, Shi R, Rehse P and Lin SX (2004) Identifying androsterone (ADT) as a cognate substrate for human dehydroepiandrosterone sulfotransferase (DHEA-ST) important for steroid homeostasis: structure of the enzyme-ADT complex. *J Biol Chem* **279**:2689–2696.

Chen G, Banoglu E and Duffel MW (1996) Influence of substrate structure on the catalytic efficiency of hydroxysteroid sulfotransferase STa in the sulfation of alcohols. *Chem Res Toxicol* **9**:67–74.

Chen WT, Liu MC and Yang YS (2005) Fluorometric assay for alcohol sulfotransferase. *Anal Biochem* **339**:54–60.

Cornish-Bowden A (1995) *Analysis of Enzyme Kinetic Data* pp 118–122, Oxford University Press, Oxford.

Duffel MW and Jakoby WB (1981) On the mechanism of aryl sulfotransferase. *J Biol Chem* **256**:11123–11127.

Falany C and Roth JA (1993) Properties of human cytosolic sulfotransferases involved in drug metabolism, in *Human Drug Metabolism: from Molecular Biology to Man* (Jeffery EH ed) pp 101–115, CRC Press, Inc. Boca Raton, FL.

Falany CN (1997) Enzymology of human cytosolic sulfotransferases. *FASEB J* **11**:206–216.

Gamage NU, Duggleby RG, Barnett AC, Tresillian M, Latham CF, Liyou NE, McManus ME and Martin JL (2003) Structure of a human carcinogen-converting enzyme, SULT1A1. Structural and kinetic implications of substrate inhibition. *J Biol Chem* **278**:7655–7662.

Gamage NU, Tsvetanov S, Duggleby RG, McManus ME and Martin JL (2005) The structure of human SULT1A1 crystallized with estradiol. An insight into active site plasticity and substrate inhibition with multi-ring substrates. *J Biol Chem* **280**:41482–41486.

Ganguly TC, Krasnykh V and Falany CN (1995) Bacterial expression and kinetic characterization of the human monoamine-sulfating form of phenol sulfotransferase. *Drug Metab Dispos* **23**:945–950.

Glatt H (1997) Sulfation and sulfotransferases 4: bioactivation of mutagens via sulfation. *FASEB J* **11**:314–321.

Guex N and Peitsch MC (1997) SWISS-MODEL and the Swiss-PdbViewer: an environment for comparative protein modeling. *Electrophoresis* **18**:2714–2723.

Hsiao YS and Yang YS (2002) A single mutation converts the nucleotide specificity of phenol sulfotransferase from PAP to AMP. *Biochemistry* **41**:12959–12966.

Jones TA, Zou JY, Cowan SW and Kjeldgaard M (1991) Improved methods for building protein models in electron density maps and the location of errors in these models. *Acta Crystallogr A* **47**:110–119.

Kakuta Y, Pedersen LG, Carter CW, Negishi M and Pedersen LC (1997) Crystal structure of estrogen sulphotransferase. *Nat Struct Biol* **4**:904–908.

Kakuta Y, Pedersen LC, Chae K, Song WC, Leblanc D, London R, Carter CW and Negishi M (1998) Mouse steroid sulfotransferases: substrate specificity and preliminary X-ray crystallographic analysis. *Biochem Pharmacol* **55**:313–317.

Laemmli UK (1970) Cleavage of structural proteins during the assembly of the head of bacteriophage T4. *Nature* **227**:680–685.

Laskowski RA, MacArthur MW, Moss DS and Thornton JM (1993) PROCHECK: A program to check the stereochemical quality of protein structures. *J Appl Cryst* **26**:283–291.

Lee KA, Fuda H, Lee YC, Negishi M, Strott CA and Pedersen LC (2003) Crystal structure of human cholesterol sulfotransferase (SULT2B1b) in the presence of pregnenolone and 3'-phosphoadenosine 5'-phosphate. Rationale for specificity differences between prototypical

SULT2A1 and the SULT2BG1 isoforms. *J Biol Chem* **278**:44593–44599.
Lu JH, Li HT, Liu MC, Zhang JP, Li M, An XM and Chang WR (2005) Crystal structure of human sulfotransferase SULT1A3 in complex with dopamine and 3'-phosphoadenosine 5'-phosphate. *Biochem Biophys Res Commun* **335**:417–423.
Marcus CJ, Sekura RD and Jakoby WB (1980) A hydroxysteroid sulfotransferase from rat liver. *Anal Biochem* **107**:296–304.
Marshall AD, Darbyshire JF, Hunter AP, McPhie P and Jakoby WB (1997) Control of activity through oxidative modification at the conserved residue Cys66 of aryl sulfotransferase IV. *J Biol Chem* **272**:9153–9160.
Marshall AD, McPhie P and Jakoby WB (2000) Redox control of aryl sulfotransferase specificity. *Arch Biochem Biophys* **382**:95–104.
Mulder GJ and Jakoby WB (1990) Sulfation in conjugation reactions, in *Drug Metabolism* (Mulder GJ and Jakoby WB eds) pp 107–161, Taylor and Francis, Ltd., London.
Otwinowski Z and Minor W (1997) Processing of X-ray Diffraction Data Collected in Oscillation Mode. *Methods Enzymol* **276**:307–326.
Pedersen LC, Petrotchenko EV and Negishi M (2000) Crystal structure of SULT2A3, human hydroxysteroid sulfotransferase. *FEBS Lett* **475**:61–64.
Petrotchenko EV, Pedersen LC, Borchers CH, Tomer KB and Negishi M (2001) The dimerization motif of cytosolic sulfotransferases. *FEBS Lett* **490**:39–43.
Raftogianis RB, Wood TC and Weinshilboum RM (1999) Human phenol sulfotransferases SULT1A2 and SULT1A1: genetic polymorphisms, allozyme properties, and human liver genotype-phenotype correlations. *Biochem Pharmacol* **58**:605–616.
Ramachandran GN and Sasisekharan V (1968) Conformation of polypeptides and proteins. *Adv Protein Chem* **23**:283–438.
Rehse PH, Zhou M and Lin SX (2002) Crystal structure of human dehydroepiandrosterone sulphotransferase in complex with substrate. *Biochem J* **364**:165–171.
Sakakibara Y, Takami Y, Nakayama T, Suiko M and Liu MC (1998) Localization and functional analysis of the substrate specificity/catalytic domains of human M-form and P-form phenol sulfotransferases. *J Biol Chem* **273**:6242–6247.
Shindyalov IN and Bourne PE (1998) Protein structure alignment by incremental combinatorial extension (CE) of the optimal path. *Protein Eng* **11**:739–747.
Sugiyama Y, Stolz A, Sugimoto M, Kuhlenkamp J, Yamada T and Kaplowitz N (1984) Identification and partial purification of a unique phenolic steroid sulphotransferase in rat liver cytosol. *Biochem J* **224**:947–953.
Thompson JD, Higgins DG and Gibson TJ (1994) CLUSTAL W: improving the sensitivity of progressive multiple sequence alignment through sequence weighting, position-specific gap

penalties and weight matrix choice. *Nucleic Acids Res* **22**:4673–4680.
Varin L and Ibrahim RK (1992) Novel flavonol 3-sulfotransferase. Purification, kinetic properties, and partial amino acid sequence. *J Biol Chem* **267**:1858–1863.
Weinshilboum R and Otterness D (1994) Sulfotransferase enzyme in conjugation-deconjugation Reactions, in *Drug Metabolism and Toxicity* (Kaufmann FC ed) pp 45–78, Springer-Verlag, Berlin.
Yang YS, Marshall AD, McPhie P, Guo WX, Xie X, Chen X and Jakoby WB (1996) Two phenol sulfotransferase species from one cDNA: nature of the differences. *Protein Expr Purif* **8**:423–429.
Zhang H, Varlamova O, Vargas FM, Falany CN and Leyh TS (1998) Sulfuryl transfer: the catalytic mechanism of human estrogen sulfotransferase. *J Biol Chem* **273**:10888–10892.

Footnotes

This research was supported by National Science Council, Taiwan, under project NSC 95-2120-M-009-003 and 95-2627-B009-004.

Figure Legends

Figure 1. Structures of the loop from residues Tyr-231 to Gly-252 of SULT2A1/PAP, SULT2A1/DHEA and SULT2A1/ADT complexes. (A) Loop and substrate binding site. Superposition of this loop was performed between the SULT2A1/PAP (*orange*) and SULT2A1/DHEA (*green*) complex structures. The structure of SULT2A1/ADT at this region is very similar to that of SULT2A1/DHEA. The two ligands (DHEA and PAP) were colored in *red* and the proposed entrance of substrate was marked by an arrow. (B) SULT2A1/DHEA and the SULT2A1/ADT complex structures. Tyr-238 (*green*) is proposed to act as a gate residue for the substrate-binding site. The DHEA molecule was placed in two orientations and was colored in *red*; ADT molecule was colored in *blue*.

Figure 2. Binding modes of DHEA and ADT molecules in SULT2A1. Comparison of the binding modes was performed between the SULT2A1/DHEA (*red*) and the SULT2A1/ADT (*blue*) complex structures. The residues, Met-16, Ile-71 and Met-137, around the DHEA and ADT molecules were shown. DHEA showed van der Waals interactions (shown by *dotted lines*) with Met-16, Ile-71 and Met-137 with C-16, C-19 and C-12 of DHEA, respectively.

Figure 3. Superimposition of the solved structures of wild-type, M137I, and M137W SULT2A1. The crystal structures of M137I (*cyan*) and M137W (*yellow*) are superimposed to the previous solved structures, SULT2A1/DHEA (*red*) and SULT2A1/ADT (*blue*) at Met-137. The DHEA in SULT2A1 complex structure is also shown and colored in *red*.

Figure 4. Multiple sequence and structure alignment of Tyr-238 and Met-137 corresponding residues among some solved-structure cytosolic sulfotransferases. The in-position residues of Tyr-238 (upper left) of SULT2A1 complex (*red*) are Phe-247 of human SULT1A1 (*green*), Leu-247 of human SULT1A3 (*magenta*), Met-247 of mouse SULT1E1 (*orange*), Leu-249 of human SULT2B1_v1 (*cyan*). The in-position residues of Met-137 (lower middle) of SULT2A1 complex are Ala-146 of human SULT1A1, Glu-146 of human SULT1A3, Ile-146 of mouse SULT1E1, Ala-148 of human SULT2B1_v1. The substrates (two orientations on the right) of sulfotransferases are DHEA, *p*NP, dopamine, 17β-estradiol and 2-[N-cyclohexylamino] ethane sulfonic acid for SULT2A1, SULT1A1, SULT1A3, SULT1E1 and SULT2B1_v1, respectively. Superposition of these known-structure sulfotransferases was created by Combinatorial Extension (CE) (Shindyalov and Bourne, 1998), and the multiple sequence alignment was produced by ClustalW (Thompson et al., 1994).

Figure 5. Schematic illustration of SULT2A1 substrate binding orientation and inhibition modulated by Met-137 and Tyr-238. The ternary dead-end complex was conceived of presence with PAP, DHEA or ADT simultaneously. DHEA (*red*) and ADT (*blue*) compound structures are shown in one or two possible substrate binding orientations in SULT2A1 and its mutants. Tyr-238 is depicted as a gate residue modulating the release of bound substrate. Met-137 (*red* in SULT2A1/DHEA and *blue* in SULT2A1/ADT complex structures) is depicted as a stereo hindrance residue modulating the substrate binding orientation.

Table 1.

RMSD values of SULT2A1/DHEA (1J99) and SULT2A1/PAP (1EFH) complex structures[a].

Residues			RMSD (Å)		
residues No.	1J99	1EFH	Backbone	Side chain	All atoms
4-230[b]	—	—	1.20	2.03	1.69
231	Tyr	Tyr	4.16	9.56	8.16
232	Ser	Ser	6.42	8.88	7.33
233	Leu	Leu	7.36	8.50	7.95
234	Leu	Leu	6.24	5.97	6.11
235	Ser	Ser	6.39	6.55	6.44
236	Val	Val	5.63	8.58	7.05
237	Asp	Asp	6.64	9.80	8.37
238	Tyr	Tyr	7.00	8.48	8.02
239	Val	Val	6.18	8.43	7.23
240	Val	Val	4.11	3.31	3.79
241	Asp	Asp	2.04	4.36	3.40
242	Lys	—[c]	—	—	—
243	Thr	—[c]	—	—	—
244	Gln	Gln	6.26	6.18	6.22
245	Leu	Leu	6.59	8.72	7.73
246	Leu	Leu	6.51	8.84	7.76
247	Arg	Arg	5.79	8.44	7.58
248	Lys	Lys	7.41	5.18	6.27
249	Gly	Gly	9.63	0	9.63
250	Val	Val	9.61	11.52	10.47
251	Ser	Ser	8.69	11.75	9.82
252	Gly	Gly	6.05	0	6.05
253-279[b]	—	—	0.98	2.34	1.83
Average			2.13	2.86	2.54

[a] Superposition of these two known structures was created by Combinatorial Extension (CE) (Shindyalov and Bourne, 1998) and the root-mean-square deviation (RMSD) was calculated by Swiss-Pdb Viewer (Guex and Peitsch, 1997).

[b] The average RMSD of these residues is less than 2.5 Å.

[c] Structure in this region was not solved.

Table 2.

Rate constants of SULT2A1 wild type and mutants using DHEA and ADT as substrates[a].

SULT2A1	DHEA				ADT			
	K_m	V_{max}	V_{max}/K_m	K_i	K_m	V_{max}	V_{max}/K_m	K_i
	μM	*nmole/min/mg*		*μM*	*μM*	*nmole/min/mg*		*μM*
Wild type	2.5 ± 0.7	227 ± 42	91	6.1 ± 1.7	1.4 ± 0.8	203 ± 86	145	0.7 ± 0.4
Y238A	3.3 ± 0.3	191 ± 8.3	58	45 ± 4.9	1.4 ± 0.1	55 ± 1.3	39	—[b]
Y238F	1.1 ± 0.2	108 ± 8.2	98	12 ± 1.7	1.5 ± 0.6	134 ± 38	90	2.2 ± 0.9
Y238W	0.7 ± 0.1	71 ± 5.1	101	15 ± 2.9	0.7 ± 0.6	79 ± 44	113	1.2 ± 0.8
M137I	1.3 ± 0.2	68 ± 4.9	52	36 ± 6.8	0.2 ± 0.06	42 ± 5.1	208	20 ± 7.9
M137V	1.9 ± 0.6	70 ± 8.9	37	53 ± 19	0.7 ± 0.3	60 ± 12	86	7.8 ± 3.2
M137W	1.3 ± 0.6	112 ± 32	86	7.1 ± 3.7	0.6 ± 0.2	61 ± 14	52	3.8 ± 1.6
M137K	ND[c]	ND[c]	ND[c]	ND[c]	ND[c]	ND[c]	ND[c]	ND[c]
M137I/Y238A	3.6 ± 0.7	48 ± 3.9	13	170 ± 53	1.4 ± 0.3	30 ± 1.8	22	159 ± 38
M137V/Y238A	6.5 ± 1.1	62 ± 4.0	9.5	466 ± 140	3.6 ± 0.4	37 ± 0.9	10	—[b]
M137W/Y238A	4.2 ± 0.3	97 ± 1.8	23	—[b]	2.0 ± 0.3	63 ± 2.2	31	—[b]
M137K/Y238A	ND[c]	ND[c]	ND[c]	ND[c]	ND[c]	ND[c]	ND[c]	ND[c]
V260E[d]	1.6 ± 0.4	160 ± 26	100	7.1 ± 1.9	1.4 ± 0.8	176 ± 74	126	1.2 ± 0.7
Y238A/V260E[d]	2.2 ± 0.1	144 ± 4.3	66	55 ± 4.8	1.8 ± 0.2	48 ± 1.4	27	—[b]

[a] Sulfotransferase activity was measured as indicated under “Experimental Procedures.”

[b] Not applicable (substrate inhibition was not observed).

[c] Not determined due to undetectable or low level of activity.

[d] Monomer mutant of SULT2A1.

Table 3.

Dissociation constants of PAP, DHEA, and ADT in wild-type and mutated SULT2A1[a].

SULT2A1	Binary complex[b]	Ternary complex[c]	
	PAP	DHEA	ADT
	nM	*μM*	*μM*
Wild type	40.7 ± 8.2	0.8 ± 0.05	0.4 ± 0.04
Y238A	48.7 ± 8.6	6.9 ± 0.3	3.2 ± 0.1
M137I	44.2 ± 8.4	1.9 ± 0.3	0.4 ± 0.06
M137W	49.2 ± 7.8	0.6 ± 0.07	0.3 ± 0.03
M137I/Y238A	32.2 ± 7.3	7.2 ± 0.4	2.4 ± 0.4
M137W/Y238A	49.4 ± 8.1	3.7 ± 0.6	2.3 ± 0.4

[a] Dissociation constants were determined with spectrofluorimeter as indicated under "Experimental Procedures."

[b] The dissociation constants of binary complex were determined with PAP (5 to 365 nM) and SULT2A1 (100 nM).

[c] The dissociation constants of ternary complex were determined with DHEA (0.1 to 50 μM) or ADT (0.1 to 50 μM) and SULT2A1 (0.5 μM) in the presence of PAP (1 μM).

Table 4.

Rate constants of SULT1A1, SULT1A3 and their mutants[a].

Enzyme		Substrate	K_m	V_{max}	V_{max}/K_m	K_i
			μM	*nmole/min/mg*		*uM*
SULT1A1	Wild type	*p* -Nitrophenol	2.2 ± 1.0	323 ± 116	147	0.8 ± 0.4
	F247A		3.2 ± 0.8	1437 ± 217	449	9.4 ± 2.1
SULT1A3	Wild type	Dopamine	6.8 ± 0.9	623 ± 30	92	174 ± 23
	L247A		22 ± 1.2	1149 ± 32	52	282 ± 22
	L247Y		36 ± 14	1669 ± 457	46	61 ± 26

[a] Sulfotransferase activity was measured as indicated under “Experimental Procedures.”

Table 5.

Data collection and structure refinement statistics

	M137I/ADT	**M137W/ADT**
Crystal data collection	BL13B1/NSRRC	BL13B1/NSRRC
Wavelength (Å)	1.000	1.000
Temperature (K)	110	110
Space group	$P2_12_12$	$C222_1$
Unit-cell parameters (Å)		
a	76.28	109.41
b	131.72	133.02
c	44.55	76.30
Resolution range (Å)	30-2.59 (2.73-2.59)	30-3.0 (3.12-3.0)
No. of unique reflections	14606	11368
Completeness (%)	99.6 (99.3)	99.4 (97.7)
$I/\sigma_{(I)}$	42.5 (10.1)	19.5 (2.8)
Average redundancy	14.2	7.8
R_{sym} (*I*) (%)[a]	6.6 (30.6)	11.4 (70.0)
No. of proteins / A.U.	1	1
Refinement and statistics		
Resolution range (Å)	20-2.6	20-3.0
Number of reflections[b]	14138	10882
Number of total atoms	2,269	2,369
R_{work} (%)[c]	22.5	24.6
R_{free} (%)[d]	26.3	30.2
Average B-factors (Å^2)	46.46	72.11
R.m.s.d from ideal values		
Bond length (Å)	0.006	0.008
Bond angles (^{o})	1.22	1.39
Dihedral angles (^{o})	21.45	22.22
Improper torsion angles (^{o})	0.752	0.848

[a] $R_{sym} = \Sigma_h \Sigma_i [| I_i (h) - \langle I (h) \rangle | / \Sigma_h \Sigma_i I_i (h)]$, where I_i is the *i*th measurement and $\langle I (h) \rangle$ is the weighted mean of all measurements of I(h).

[b] Reflections of $2\sigma_I$ cutoff were applied in generating the refinement statistics.

[c] $R_{work} = \Sigma_h | F_o - F_c | / \Sigma_h Fo$, where Fo and Fc are the observed and calculated structure factor

amplitudes of reflection h.
[d] R_{free} is as R_{work}, but calculated with 10% pf randomly chosen reflection omitted from the refinement.
[e] ESD, estimated standard deviation.
[f] Ramachandran plot outliers are all glycine.

Effect of metal binding and posttranslational lysine carboxylation on the activity of recombinant hydantoinase

Cheng-Yang Huang, Ching-Chen Hsu, Mei-Chun Chen
Department of Biological Science and Technology, National Chiao Tung University, Hsinchu, Taiwan

Yuh-Shyong Yang(✉)
Department of Biological Science and Technology, National Chiao Tung University;
Instrument Technology Research Center and National Nano Device Laboratories, National Applied Research Laboratories, Hsinchu, Taiwan
e-mail: ysyang@faculty.nctu.edu.tw;
Fax: 886-3-5729288.

Bacterial hydantoinase possesses a binuclear metal center in which two metal ions are bridged by a posttranslationally carboxylated lysine. How the carboxylated lysine and metal binding affect the activity of hydantoinase was investigated. A significant amount of iron was always found in *Agrobacterium radiobacter* hydantoinase purified from unsupplemented cobalt, manganese or zinc amended *Escherichia coli* cell cultures. A titration curve for the reactivation of apo-hydantoinase with cobalt indicates that the first metal was preferentially bound but did not give any enzyme activity until the second metal was also attached to the hydantoinase. The pH profiles of the metal-reconstituted hydantoinase were dependent on the specific metal ion bound to the active site, indicating a direct involvement of metal in catalysis. Mutation of the metal binding site residues, H57A, H59A, K148A, H181A, H237A, and D313A, completely abolished hydantoinase activity but preserved about half of the metal content except for K148A that lost both metals in its active site. However, the activity of K148A could be chemically rescued by short-chain carboxylic acids in the presence of cobalt, indicating that the carboxylated lysine was needed to coordinate the binuclear ion within the active site of hydantoinase. The mutant D313E enzyme was also active but resulted in a different pH profile as compared to that of wild-type hydantoinase. A mechanism for hydantoinase involving metal, carboxylated K148 and D313 was proposed.

Key words:
Hydantoinase, metalloenzyme, carboxylated lysine.

INTRODUCTION

Hydantoinase (EC 3.5.2.2) is a metalloenzyme widely distributed in living organisms and was first described in the 1940s as occurring in plants and animals [1,2]. In the 1950s, the enzyme isolated from calf liver was shown to catalyze the hydrolysis of dihydrouracil and dihydrothymine and was known as dihydropyrimidinase [3]. Due to their broad substrate specificities, hydantoinase and dihydropyrimidinase were also classified as imidases [4]. Imidases from bacteria and mammals are generally known as hydantoinase and dihydropyrimidinase, respectively [5]. Hydantoinase catalyzes the reversible hydrolytic ring opening of six-membered or five-membered cyclic imides such as dihydropyrimidines and 5'-monosubstituted hydantoins to the corresponding 3-ureido acids and carbamoyl amino acids, respectively [6]. Hydantoinase also plays a role in industry for the preparation of optically active compounds [7-9]. Hydantoinase is used in combination with carbamoylase as biocatalysts for the enantiospecific enzymatic production of non-proteinogenic amino acids from racemic hydantoins [7,8]. The products are valuable precursors for the production of β-lactam antibiotics or synthetic peptides.

On the basis of an analysis of the amino acid sequences, hydantoinase was suggested to belong to the group of metal-dependent amidohydrolases [10]. Members of this family contain either mononuclear metal center or binuclear metal center [10]. For some bimetal-containing amidohydrolases, such as dihydroorotase [11], urease [12], and phosphotriesterase [13], their metal ions were found to be bridged by a carboxylated lysine ligand. The crystal structures of hydantoinase from *Burkholderia pickettii* [14], *Thermus* sp. [15], and *Bacillus stearothermophilus* [16] were resolved, and a carboxylated lysine located within the active site was also observed to bridge the two metals (Fig. 1). Recently, the crystal structure of hydantoinase from *Bacillus* sp. AR9 was determined; however, the usual posttranslational carboxylation of the active site lysine residue was not found [17]. These observations raise an interesting question as to why the lysine needs to be carboxylated for hydantoinase and its effect on metal binding and enzyme activity. In this report, we examined the metal contents and characterized the effects of metal binding on the activity of recombinant hydantoinase from *Agrobacterium radiobacter* by site-directed mutagenesis on specific amino acids involved in metal binding. The importance of the posttranslational modification of the carboxylated lysine was studied by using short chain carboxylic acids for the chemical rescue of the mutant K148A.

MATERIALS AND METHODS

Materials

The resistance of water used was more than 18 MΩ, which was purified by reverse osmosis followed by passage through a Millipore Reagent Water System (Millipore). Candidate substrates for hydantoinase, such as barbituric acid, allantoin, dihydroorotate, uracil, pyromellitic diimide, phthalic anhydride, 5-bromouracil, 2,3-naphthalene-dicarboximide, 1,8-naphthalimide, 3,4,5,6-tetrachlorophthalimide, 4-amino-1,8-naphthalimide, 2*H*-1,3-benzoxazine-2,4(3*H*)dione, biuret, bemegride, 5,5-dimethyl-hydantoin, uridine, 5-ethyl-methyl-hydantoin, parabanic acid, rhodanine, 2,4-thiazolidinedione, *N*-methylmaleimide, *N*-cyclohexylmaleimide, and oxindole, were obtained from Aldrich (U.S.A.). DEAE Sepharose, chelating Sephacel (fast flow), and HiTrap™ desalting column were purchased from GE Healthcare Bio-Sciences (U.S.A.). Bis-Tris propane, sodium acetate, PMSF, 8-HQSA and EDTA were purchased from Sigma (U.S.A.). Sodium chloride, sodium hydroxide, potassium phosphate, glycine, sodium dodecyl sulfate (SDS) and zinc acetate were obtained from J. T. Baker (U.S.A.). All other reagents were of the highest grades commercially available.

Enzyme assay

A rapid spectrophotometric assay [4] was used as the standard assay. Briefly, the decrease in absorbency at 298 nm was measured upon hydrolysis of phthalimide as the substrate at 25 °C. To start the reaction, the purified hydantoinase (5-100 μg) was added into a 1 ml solution, containing 1 mM phthalimide and 100 mM Tris-HCl at pH 7.9. Under these conditions, a change in A_{298} of 2.26 represents the hydrolysis of 1 μmol of the substrate. The hydrolysis of the substrate was monitored with a UV/Vis spectrophotometer (Hitachi U 3300). The hydrolysis of a number of candidate substrates was assayed spectrophotometrically in an entirely similar manner except for the wavelength used; necessary modifications of the assay were needed for specific compounds. The extinction coefficient of each substrate was determined experimentally by direct measurement with a spectrophotometer.

Protein concentration

The protein concentrations of enzyme solution were determined by BCA protein assay (Pierce, USA) using bovine serum albumin as a standard.

Expression and purification of recombinant hydantoinase

The procedure for the purification of recombinant *Agrobacterium radiobacter* hydantoinase and its mutant proteins was modified according to a previous report [18]. Total hydantoinase activities in cell cultures grown in zinc, cobalt, or manganese ions (range from 0 to 5 mM) were determined and the maximal activities were obtained at 1 mM metal ion concentration. Cell growth was inhibited by these metal ions at concentration above 2 mM. Thus, metal ions at 1 mM concentration were amended for cell culture and for routine purification of hydantoinase.

E. coli BL21 (DE3) cells were transformed with plasmid pHDT200 and grown in LB medium supplemented with 50 μg of ampicillin per ml plus metal ion (1 mM zinc chloride, cobalt chloride, manganese chloride, nickel chloride, or cadmium chloride) at 37 °C with rapid shaking. When the cultures (500 ml) reached an A_{600} of 0.6, IPTG was added to 50 μM, the temperature of flasks was shifted to 25 °C, and growth continued for an additional 25 hours. Cells were chilled on ice, harvested by centrifugation, and frozen at -80 °C. After thawing, cells were resuspended in 20 mM Tris-HCl buffer (pH 7.9) and disrupted by sonication (the power was set at 3.5; each pulse lasted 2 secs, waited 2 secs between pulses and continued for 5 minutes; the complete pulse sequence was repeated three times) with ice

cooling between pulses. The disrupted cell suspensions were centrifuged at 50,000g for 30 min. The supernatant solutions were chromatographed with DEAE Sepharose HR 10/16 column (GE Healthcare Bio-Sciences). After being washed with 20 mM Tris-HCl (pH 7.9), hydantoinase was eluted with a 0 to 0.3 M NaCl gradient in 20 mM Tris-HCl (pH 7.9) in a total volume of 500 ml. Fractions were examined for the presence of hydantoinase protein by SDS-PAGE analysis, and those containing enzyme of sufficient purity were pooled and directly applied to a column (1.6-cm diameter by 10 cm; GE Healthcare Bio-Sciences) of chelating Sephacel (fast flow) that was treated with five times gel volume containing 0.2 M zinc acetate and then equilibrated with buffer A (20 mM Tris and 0.5 M NaCl, pH 7.0). The loaded column was washed with 100 ml buffer A. The enzyme was then eluted with a linear glycine gradient from 0 to 1 M with buffer A and buffer A plus 1 M glycine in 500 ml. The fractions were examined by SDS-PAGE analysis, and those containing greater than 95% pure hydantoinase were pooled, dialyzed against the dialysis buffer (20 mM Tris-HCl, pH 8.0) with two buffer changes, and concentrated to ~10 mg/ml. The mutant proteins could be purified to homogeneity in a manner similar to native hydantoinase. In general, about 10 mg purified hydantoinase (or mutant protein) was obtained per 0.5 liter cell culture.

Preparation of apo-hydantoinase

The preparation of apo-form of the hydantoinase was according to the published procedure [19]. Briefly, purified enzyme (10 mg/ml; 10-15 ml) was dialyzed against a chelating buffer (pH 6.5) that contained MES (50 mM) and 8-HQSA (15 mM) at room temperature for 2 days. The enzyme solution was dialyzed against HEPES buffer (pH 7.0, 10 mM) at 4 °C for 4 hours, and then passed through a HiTrap^{TM} desalting column and eluted with HEPES buffer (pH 7.0, 10 mM) at 4 °C. The activity of the resultant enzymes (apo-hydantoinase) detected by the standard assay was less than 0.4% of that of Co-reconstituted enzyme and the metal content was about 0.01 to 0.09 mol of zinc, manganese, cobalt and iron per mol of the enzyme monomer according the Inductively Coupled Plasma-Mass Spectrometry (ICP-MS) (Elan 5000, Perkin Elmer, USA). The apo-hydantoinase was stored at 4 °C and was stable for a minimum of a month.

Preparation of metal-reconstituted hydantoinase

The reconstitution of apo-enzymes with metal ion was according to the published procedure [19]. The apo-enzyme (10 mg/ml in 4 ml) was dialyzed at 4°C for 2 days in HEPES buffer (4L, 10 mM at pH 7) plus one of the following metal ions (1 mM): Co^{2+}, Mn^{2+}, or Zn^{2+}. The approximate time for recovery of the maximum enzymatic activity under the condition was about 40 ± 5, 30 ± 5, and 10 ± 2 min for the Co^{2+}, Mn^{2+}, and Zn^{2+}, respectively. ICP-MS was used to measure the concentration of each cation in the protein samples. Prior to the performance of ICP-MS analysis, the protein solution was passed through a HiTrap^{TM} desalting column eluted with HEPES buffer (pH 7.0, 10 mM) at 4 °C to remove excess metal ions in the protein solution. Measurements for each sample were repeated five times and the standard deviation was calculated. Normally, two or more samples were used for each determination by ICP-MS. Less than 1 ml enzyme sample (0.05-0.2 mg/ml) was used for each determination.

The pH profiles

The K_m and k_{cat} of the enzymatic reaction was determined over the pH range of 5.5-9.5. The reaction was buffered with 0.1 M sodium acetate (pK_a = 4.8) and 0.1 M Bis-Tris propane (pK_as = 6.8 and 9.0) in desired pH, and appropriate amounts of the enzyme (about 5-400 μg) were added to start the reaction. The pH of buffers was determined at 25 °C. K_m and k_{cat} were obtained by nonlinear regression (Enzyme Kinetics module of SigmaPlot) using 10-15

measurements determined at different substrate concentrations. Reaction rates obtained at each pH value were fitted to the following equation using Sigma-Plot, $(V_{max})_H=V_{max}K_a/K_a+[H^+]$, then p$K_a$ value was given, where $(V_{max})_H$ is the maximal degradative reaction rate at a particular pH; V_{max} is the maximal rate when all the enzyme sites are in the appropriate ionic form, and is used to represent the k_{cat}; K_a is the acid dissociation constant for a catalytic residue at the active site [20]. A plot of k_{cat}/K_m or K_m as a function of pH was also fitted to this equation in a similar manner.

Site-directed mutagenesis

Each hydantoinase mutant was generated according to the Stratagene QuickChange mutagenesis protocol (Stratagene, La Jolla, CA) using the plasmid pHDT2000 as the template [18]. Each mutant was confirmed by nucleotide sequencing. Expression and purification of the mutant proteins were the same as described for wild-type hydantoinase protein. The oligonucleotide primers for the preparation of mutants were GGCATCGACGTTGCTACGCATGTCGAG and CTCGACATGCGTAGCAACGTCGATGCC for H57A; ATCGACGGTCATACGGCTGTCGAGACGGTC and GACCGTCTCGACAGCCGTATGAACGTCGAT for H59A; AGCCATGAAGACCGCGAAGGAGGTGATGCC and GGCATCACCTCCTTCGCGGTCTTCATGGCTTA for K148A; GCGATAAGCCATGAAGACACAGAAGGAGGTG and GGCATCACCTCCTTCTGTGTCTTCATGGCTTA for K148C; GCGATAAGCCATGAAGACATCGAAGGAGGTG and GGCATCACCTCCTTCGATGTCTTCATGGCTTA for K148D; GCGATAAGCCATGAAGACCGAGAAGGAGGTG and GGCATCACCTCCTTCTCGGTCTTCATGGCTTA for K148S; CTCGTCATGGTGGCCGCGGAGAACGGC and GCCGTTCTCCGCGGCCACCATGACGAG for H181A; GCCCCGATCTACATCGTGGCTCTGACCTGCG and TTCTTCGCAGGTCAGAGCCACGATGTAGAT for H237A; CTCGAAACGGTCTCCTCGGCCCATTGTTCCT and GAGCCAGGAACAATGGGCCGAGGAGACCGT for D313A; CTCGAAACGGTCTCCTCGGAGCATTGTTCCT and GAGCCAGGAACAATGCTCCGAGGAGACCGT for D313E. The underlined sequences denote the mutated amino acids.

RESULTS

Metal contents and activities of recombinant hydantoinase

The addition of divalent metal ions to the standard growth medium was found to substantially increase the hydantoinase activity. Metal contents and activities of hydantoinase purified from unsupplemented zinc-, cobalt-, and manganese-amended cultures and are shown in Table 1. Cadmium and nickel ions were also tested as supplements but the resulting hydantoinase activity was similar to that from unsupplemented medium.

Mixtures of metals were found in a purified hydantoinase as shown in Table 1. Significant amounts of iron, zinc and manganese were observed in recombinant hydantoinase obtained from cell culture without supplementing additional metal ions. It was also determined that the metal contents for Zn, Fe, Mn, Co and Ni were 12.7±0.06, 6.66±0.19, 0.34±0.004, 0.19±0.004 and 0.02±0.003 μM, respectively, in unsupplemented cell culture. The total metal contents (for Zn, Co, Mn and Fe) in recombinant hydantoinase were near to 2 and 1.6 per enzyme subunit for purified hydantoinase obtained from metal-amended and unsupplemented media (Table 1), respectively. Interestingly, zinc, presumably the native metal ion in hydantoinase, was neither the major metal found in recombinant hydantoinase from unsupplemented medium nor the metal to give the highest hydantoinase activity (Table 1). The results about metal contents in recombinant hydantoinase shown in Table 1 indicate that preparation of apo-hydantoinase and reconstitution of the apo-hydantoinase with metals were needed for the proper understanding of the metal effect on catalytic properties of recombinant hydantoinase.

Reactivation of apo-hydantoinase

A titration curve for the reactivation of apo-hydantoinase with cobalt is shown in Fig. 2a. This plot shows a slow increase in hydantoinase activity at low metal ion content (less than 1 cobalt per enzyme subunit) followed by a sharp increase in hydantoinase activity that reached maximal activity when the ratio of metal to protein was equal to 2. A kinetic model (Fig. 2b) for metal-activation of apo-hydantoinase was proposed for the non-linear increase in catalytic activity with an increasing ratio of cobalt to protein as shown in Fig. 2a. It was suggested that in this model only protein with a fully assembled binuclear metal center (M_1M_2-hydantoinase) was catalytically active and the first metal (M1) was preferentially bound to the binuclear center. It was unlikely that metal-binding of apo-hydantoinase occurred in cooperative manner. In such a case, the metal would have been preferentially bound in pairs and a plot with a linear increase in catalytic activity would have been observed. Thus, the binding of the first metal ion to apo-hydantoinase was proposed to be tighter than that of the second metal ion.

The reconstitution of apo-hydantoinase with different divalent metal ions resulted in a differential recovery of catalytic activity as shown in Table 1. The metal-reconstituted hydantoinase gave significantly higher specific activities than those of enzyme purified directly from metal-amended cultures. Incubation of apo-hydantoinase with Cd^{2+} and Ni^{2+} did not significantly enhance hydantoinase activity. The metal content per subunit enzyme was 2.6±0.1, 2.5±0.1, and 2.8±0.1 for Co-, Zn-, and Mn-reconstituted hydantoinase, respectively. These results indicate that the hydantoinase might have more than two metal binding sites; two of them are needed for maximal activity (Fig. 2a).

Effect of metals on the substrate specificity of hydantoinase

The kinetic constants for the metal-reconstituted hydantoinase for several representative substrates are shown in Table 2. Significant changes of K_m, k_{cat} and k_{cat}/K_m were found for each substrate with different metals in hydantoinase, which indicate that the substrate specificity of hydantoinase was metal dependent. However, the variations were all within one order of magnitude.

Effect of metals on the pH profiles of hydantoinase

The pH dependence of enzyme activity and catalytic efficiency (k_{cat}, and k_{cat}/K_m) of the metal-reconstituted hydantoinase was determined (figures of the pH profiles are given as supporting information). Metal ions appeared to play a significant role on enzyme function. Both k_{cat} and k_{cat}/K_m were notably influenced by the variation in metal ions in the optimal pH range. According to the pH profiles, a general-base catalyzed reaction of the hydantoinase was expected, and a group within the active site of hydantoinase must be ionized for catalytic activity. The kinetic pK_as of the Co-, Zn-, and Mn-reconstituted hydantoinase derived from pH profiles were 6.3±0.1, 6.0±0.1, and 6.6±0.1, respectively, for k_{cat}; 7.0±0.1, 6.7±0.1, and 6.8±0.1, respectively, for k_{cat}/K_m. These results reflect that ionization of the active site functional group was dependent on the specific metal ion bound to the binuclear metal center.

Mutational analysis for the metal binding site

The role of conserved residues (as shown in Fig. 1) for metal binding of hydantoinase was probed by site-directed mutagenesis, and the metal content and specific activity of the hydantoinase mutants are listed in Table 3. As expected, the catalytic activities for these mutant proteins were severely impaired. Only D313E was found to be active, and its specific activity was about 20-fold less than that of wild-type hydantoinase. D313E also contained about 2 metals per enzyme subunit (Table 3). K148 mutants (K148A, K148C, K148D, K148S), unable to possess a carboxylated side-chain, were found to have 0.5-0.9 metal per enzyme subunit, less than those of other mutants. Other mutant proteins (H57, H59, H181 and H237 shown in Table 3) were found to possess 1.2 to 1.4 metals per subunit. Results shown in Table 3 indicate that the binuclear metal center was essential for the catalytic activity of hydantoinase. These data were in agreement with the titration curve and proposed model presented in Fig. 2 that only the M_1M_2-hydantoinase form was active.

Chemical rescue of K148A by short-chain carboxylic acids

In the presence of a high concentrations of cobalt (5 mM), the K148 mutants, K148A, K148C, K148S, and K148D, were activated to values of 1.4, 4.9, 1.6, and 0.7 $x10^{-3}$ μmol/min/mg, respectively. Addition of a short-chain carboxylic acid, such as acetic acid, propionic acid, or butyric acid, into the reaction mixtures further improved the activity of K148A by nearly two orders of magnitude as shown in Fig. 3. High concentrations of short chain carboxylic acids, 45, 40 and 35 mM for acetic acid, propionic acid and butyric acid, respectively, were needed to give the maximal activity of K148A. Taken together, the studies of mutational analysis and chemical rescue for K148 indicate that the posttranslational modification of carboxylated Lys148 was essential for binuclear metal coordination and assembly of active site of hydantoinase.

Dual Roles of D313 in metal binding and catalysis

In contrast to D313A, D313E maintained 2 metals per subunit and exhibited enzyme activity (Table 3). The pH dependence of D313E (Fig. 4) was found to differ from those of wild-type hydantoinase. The kinetic pK_as of D313E derived from Fig. 4 were 6.7 ± 0.1 and 7.4 ± 0.1 for k_{cat} and k_{cat}/K_m, respectively, which were significantly higher (0.4 and 0.7, respectively) than those of wild-type hydantoinase. These observations from site-directed mutagenesis and associated kinetic data indicated that D313 had dual roles in both metal binding and in catalysis.

DISCUSSION

It is interesting to observe that iron appeared to be the most favorable metal ion of recombinant *Agrobacterium radiobacter* hydantoinase expressed in *Escherichia coli*. Significant amounts of iron were found in the recombinant hydantoinase even when a large excess of Zn, Co or Mn metal ion was added in the cell culture (Table 1). However, unlike other iron enzymes, such as cytosine deaminase [22], methionine aminopeptidase [23], and deformylase [24], iron did not activate apo-hydantoinase activity. It has been observed that recombinant hydantoinase exhibits no enzyme activity without supplementing with a large excess of active metal ions, and metal-reconstituted hydantoinase exhibits higher enzyme activity [19]. At that time, the occupation of metal binding site by iron was not suspected. The results shown in Table 1 clearly explained why metal supplementation in the cell culture was needed to obtain active recombinant hydantoinase and why metal-reconstituted hydantoinase exhibited higher enzymatic activity. Both zinc and iron are the most abundant and important metal nutrients for growth of bacteria [25]. It is unclear why iron is the preferred metal incorporated into recombinant hydantoinase and why the highest activity of hydantoinase is observed when the cell cultures are supplemented with cobalt. It is unlikely that cobalt has a biological role *in vivo* because of its low bioavailability in the cell [25].

Both the metal titration (Fig. 2) and metal contents (Tables 1 and 3) for bacterial hydantoinase suggest that there are two metal ions within the active site needed for hydantoinase activity. However, significantly higher metal content (about 2.5 metals per enzyme subunit) were determined in highly active metal-reconstituted hydantoinase (Table 3). It was not surprising that additional metal binding sites on the protein surface were available because hydantoinase could efficiently bind to a chelating column (described in MATERIALS and METHODS section for protein purification). Dihydroorotase has been found to have nearly three metals per monomer [26]. The recent crystal structure of *Bacillus* sp. hydantoinase reveals that there is a third metal binding site near the binuclear active site of the enzyme [17]. The significant amounts of metals found in K148 mutants (their carboxylated sites were eliminated) and more than two metals per subunit found in wild-type hydantoinase (Table 3) indicate the presence of extra metal binding sites in addition to the binuclear active site. The metal center in the amidohydrolase superfamily is vital for enzyme activity [27] and a mononuclear or binuclear metal center is the structural landmark for hydrolytic enzymes with the TIM-barrel structural fold (named after triosephosphateisomerase consisting of eight α-helices and eight parallel β-strands that alternate along the peptide backbone) [28]. Mutation of each of the amino acids of the binuclear metal center (Fig. 1) partially eliminated a metal binding site as presented in Table 3. The above observations regarding metal contents might also reconcile the seemingly contradictory data reported previously [29] for the possibility of metal contamination in recombinant hydantoinase. Metal quantitation indicates that only a mutation at lysine could eliminate the binding of nearly two metals (K148A) as compared to wild-type hydantoinase. This finding is consistent with the crystal structure shown in Fig. 1 and indicates that posttranslational lysine caboxylation is necessary for binuclear metal binding.

Hydantoinase of bacterial origin and its mammalian counterpart, dihydropyrimidinase, exhibit a broad substrate spectrum [4]. As shown in Table 2, the K_m's of the three representative substrates are high in the mM ranges, especially for those of dihydrouracil. Variation of the active-site metal center kept the K_m's within the same order of magnitude, but the K_m's of mammalian dihydropyrimidinase are one order of magnitude lower than those of bacterial enzymes using dihydropyrimidine and 6-methyldihydropyrimidine as substrate [4], which suggests that the mammalian dihydropyrimidinase has its important biological role in the reductive degradation of pyrimidine degradation. The specific biological function of hydantoinase in bacteria is unclear [5].

The sizes of the metal have been proposed as the factors that affect the activity of hydantoinase [19]. In Table 2, the effect of metal on the substrate specificity of hydantoinase was examined for three representative substrates, one six-membered ring dihydropyrimidine, one bicyclic phthalimide and a five-membered ring hydantoin. The results indicate that the metal ion not only affected the activity of hydantoinase but also significantly affected its substrate selectivity. The differences in catalytic efficiency (k_{cat}/K_m) between the best and worst substrates tested were 10-, 52- and 178-old for Zn, Co and Mn, respectively, in the metal-reconstituted hydantoinases. This indicates that Zn-hydantoinase gave less discrimination between dihydrouracil and 5-leucinyl-hydantoin, while Mn-hydantoinase saw dihydrouracil and 5-leucinyl-hydantoin as two very distinct substrates.

Activity of K148A could be chemically rescued by small organic acids in the presence of high concentration of metal ions (Fig. 3), and smaller carboxylic acids lead to better hydantoinase activity (acetate > propionate > butyrate) (Fig. 3). The variation may be due to the accessibility of the carboxylic acids to the active site. The maximal activity of K148A was still 10-fold less than that of wild-type hydantoinase (Table 3 and Fig. 3). One of the reasons for the difference in hydantoinase activity might be because carbamate and carboxylate are different in chemical properties as shown in Figs. 5a and 5b. A resonance structure of carbamate gives both oxygen atoms of a carbamate formal negative charges (Fig. 5a) perhaps promoting the bimetal binding (31,32). A partially positive charge, which is not available for carboxylate (Fig. 5b), is also formed in carbamate resulting from lysine carboxylation. This structural feature for the active sites of phosphotriesterase [13], urease [12], dihydroorotase [11], and isoaspartyl dipeptidase [30] is very similar to that of hydantoinase. A combination of site-directed mutagenesis and chemical rescue studied for phosphotriesterase [33] gives similar results to those of hydantoinase reported in this study. In contrast, chemical rescue for another carbamate-dependent enzyme, RUBISCO, not a member of the amidohydrolase superfamily, was not successful [35], suggesting that the role of carbamate in RUBISCO may be not as the same as phosphotriesterase and hydantoinase. Other zinc-amidohydrolases, such as dihydroorotase and allantoinase, contain carbamated-lysine and catalyze similar reactions [21,27,36]. However, the titration curve for addition of the metals into the active site of phosphotriesterase indicates a cooperative manner for assembly of the binuclear metal center [34], different from our study on hydantoinase (Fig. 2). The titration curve for the reactivation of apo-hydantoinase indicates that the first metal was preferentially bound but did not give any enzyme activity until the second metal was also bound to the hydantoinase. The relative binding affinities of the two metal binding sites for cobalt were roughly estimated to be 5:1 according to the slopes of the metal titration curve shown in Fig. 2a. It is however difficult to determine which is the preferred binding site (α or β as shown in Fig. 1). A mutagenesis study (Table 3) showed that either metal binding site can be occupied by cobalt with the removal of the metal ligand by site-directed mutagenesis in the other metal binding site. It is interesting to observe that D313, which coordinates to the α metal (Fig. 1), can be replaced with glutamate and retain full metal binding capacity (Table 3). It appears that the α metal may be the preferred one when both metal binding sites are available.

Variations in pK_a values with different metal ions in hydantoinase indicate that ionization of the active site functional groups is dependent on the specific metal binding to the binuclear metal center. As shown in Figure 5c, metal ions are proposed to directly promote the activation of the hydroxyl group for the nucleophilic attack on hydantoin. Asp313 was proposed to be involved in the coordination of metal and activation of the hydroxyl group. The pK_a values of k_{cat}, 6.3±0.1, 6.0±0.1, and 6.6±0.1 for Co-, Zn-, and Mn-reconstituted hydantoinase, respectively, indicate that the pK_a of hydroxyl group activated by metal ion (Fig. 5c) may be significantly affected by the metal ion in the active site. The pK_a values of k_{cat}/K_m, 7.0±0.1, 6.7±0.1, and 6.8±0.1 for Co-, Zn-, and Mn-reconstituted hydantoinase, respectively,

indicates that the overall catalytic efficiency, which includes substrate binding, may be affected in a different manner. In Fig. 5c, Asp313 is shown to coordinate one metal ion (α) and to function as a base to stabilize the hydroxyl group activated by other metal ion (β) and to stabilize the intermediate, the dihydroxyl hydantoin (not shown) following the nucleophilic attack by the hydroxyl group. The pK_a values obtained with the D313E mutant (Fig. 4) were significantly higher (0.4 and 0.7 for k_{cat} and k_{cat}/K_m, respectively) than those of wild-type hydantoinase, which supported the mechanism shown in Fig. 5c that D313 is directly involved in the metal assisted imide hydrolysis and stabilization of the intermediate or transition state of hydantoin hydrolysis. The significant perturbation in active site structure would be expected with the mutation of aspartic acid to glutamate. Increase in pK_a values may indicate that glutamate is less effective to function as metal coordinator or to stabilize the transition state of the reactant in the hydantoinase active site.

The chemical mechanism of binuclear metal center containing amidohydrolase [27] is likely under three steps: (i) the hydrolytic water molecule must be activated for nucleophilic attack, (ii) the amide bond of the substrate must be made more electrophilic by polarization of the carbonyl-oxygen bond, and (iii) the leaving group nitrogen must be protonated as the carbon-nitrogen bond is cleaved. Thus, a single group must be unprotonated for the catalytic activity [37]. The respective kinetic pK_a obtained from the pH profiles of the metal-reconstituted hydantoinase varies, suggesting the deprotonation of the enzyme is associated with the specific metal bound to the active site. Moreover, based on the crystal structure of dihydroorotase [11], the bimetal ion is proposed to function as Lewis acid for polarizing the carbonyl group of the substrate. The carbonyl oxygen of the substrate directly interacting with the metal center will diminish the electron density and facilitate nucleophilic attack by the bridging hydroxide. In the final step, the amide nitrogen of the substrate must be protonated. The crystal structure of hydantoinase shows that the D313 is responsible for the proton transfer. This residue has been proposed as the group that shuttles the proton from the bridging hydroxide to and from the substrate and product during catalysis [21]. This is consistent with our finding that the kinetic pK_a values of D313E derived from the pH profile were significantly shifted when compared with those of the wild-type enzyme. The aspartate located in the active site of related amidohydrolases, phosphotriesterase [38] and dihydroorotase [39], has also been demonstrated to be involved in proton transfer reactions with the bridging hydroxide.

It has been speculated that the functionally related amidohydrolases, such as hydantoinase (dihydropyrimidinase), dihydroorotase, and allantoinase, use a similar catalytic mechanism for the hydrolysis of the cyclic amide ring [21, 29, 40]. The chemical mechanism of hydantoinase presented here was similar to that of *E. coli* dihydroorotase [39], and thus, it further raises an important question as to whether their mammalian counterparts use the same mechanism. Three lines of evidence may suggest that the difference of enzyme properties between mammalian dihydropyrimidinase and bacterial hydantoinase requires further attention. The most interesting findings in the amidohydrolase superfamily family are their metal content. Hydantoinases from bacteria and yeast are found to contain two metal ions; however, its mammalian counterparts have one metal ion [19, 47, 48 49]. Second, bacterial hydantoinase is generally EDTA-labile while its mammalian counterparts are EDTA-resistant (even above 100 mM), suggesting that bacterial hydantoinase and dihydropyrimidinase have different metal binding affinities, or the metal in dihydropyrimidinase is inaccessible to EDTA. Third, the activities of animal dihydropyrimidinases are significantly higher than those from yeast and bacteria [21, 41]. Similarly, these observations are also found for dihydroorotase. In higher organisms, dihydroorotase is found within a large polyfunctional protein CAD that contains one metal ion [42]; in bacteria such as *E. coli*, however, dihydroorotase is found to have two metal ions [11]. The one metal/two metal phenomena were observed in other

enzyme family with interesting association to the amidohydrase superfamily described above. The aminopeptidase from *Aeromonas proteolytica* contains two zinc ions in the active site and is bridged by an aspartic acid site chain [43]. This structure may highly resemble to that of K148A mutant rescued by carboxylic acids (Fig. 3). Glyoxalase II of the metallo-β-lactamase family from *Arabidopsis thaliana* is shown to bind a mixture of Zn, Fe, or Mn, but the binding of iron and zinc to this enzyme occurs exclusively as bimetal centers [44]. However, other metallo-β-lactamase from *Bacillus cereus* contains a mononuclear Zn in active site [45]. Another metallo-β-lactamase L1 from *Stenotrophomonas maltophilia* is found to contain 1 and 2 equiv of Zn and 2 equiv of Zn plus hydrolyzed nitrocefin (an antibiotic) [46]. At present, no structural data are available for mammalian dihydroorotase and dihydropyrimidinase that contain one metal per enzyme subunit.

Acknowledgement

We thank Yi-Rong Chen for purification of D313E mutant protein. This research was supported by grants from the National Science Council, Taiwan (96-2627-B-009-004).

Reference

1. Bernheim F, Bernheim MLC (1946) J Biol Chem 163:683-685
2. Eadie G, Bernheim F, and Bernheim, M.L.C. (1949) J Biol Chem 181:449-458
3. Wallach DP, Grisolia S (1957) J Biol Chem 226:277-288
4. Yang YS, Ramaswamy S. Jakoby WB (1993) J Biol Chem 268:10870-10875
5. Syldatk C, May O, Altenbuchner J, Mattes R, Siemann M (1999) Appl Microbiol Biotechnol 51:293-309
6. Vogels GD, Van der Drift C (1976) Bacteriol Rev 40:403-468
7. Schoemaker HE, Mink D, Wubbolts MG (2003) Science 299:1694-1697
8. Altenbuchner J, Siemann-Herzberg M, Syldatk C (2001) Curr Opin Biotechnol 12:559-563
9. May O, Nguyen PT, Arnold FH (2000) Nat Biotechnol 18:317-320
10. Holm L, Sander C (1997) Proteins 28:72-82
11. Thoden JB, Phillips GN Jr., Neal TM, Raushel FM, Holden HM (2001) Biochemistry 40:6989-6997
12. Jabri E, Carr MB, Hausinger RP, Karplus PA (1995) Science 268:998-1004
13. Benning MM, Kuo JM, Raushel FM, Holden HM (1995) Biochemistry 34:7973-7978
14. Xu Z, Liu Y, Yang Y, Jiang W, Arnold E, Ding J (2003) J Bacteriol 185:4038-4049
15. Abendroth J, Niefind K, Schomburg D (2002) J Mol Biol 320:143-156
16. Cheon YH, Kim HS, Han KH, Abendroth J, Niefind K, Schomburg D, Wang J, Kim Y (2002) Biochemistry 41:9410-9417
17. Radha Kishan KV, Vohra RM, Ganesan K, Agrawal V, Sharma VM, Sharma R (2005) J Mol Biol 347:95-105
18. Huang CY, Chao YP, Yang YS (2003) Protein Expr Purif 30:134-139

19. Huang CY, Yang YS (2002) Biochem Biophys Res Commun 297:1027-1032
20. Cleland WW (1979) Methods Enzymol 63:103-138
21. Gojkovic Z, Rislund L, Andersen B, Sandrini MP, Cook PF, Schnackerz KD, Piskur J (2003) Nucleic Acids Res 31:1683-1692
22. Ireton GC, McDermott G, Black ME, Stoddard BL (2002) J Mol Biol 315:687-697
23. D'Souza VM, Holz RC (1999) Biochemistry 38:11079-11085
24. Becker A, Schlichting I, Kabsch W, Groche D, Schultz S, Wagner AF (1998) Nat Struct Biol 5:1053-1058
25. Faraldo-Gomez JD, Sansom MS (2003) Nat Rev Mol Cell Biol 4:105-116
26. Washabaugh MW, Collins KD (1984) J Biol Chem 259:3293-3298
27. Seibert CM, Raushel FM (2005) Biochemistry 44:6383-6391
28. Gerlt JA, Raushel FM (2003) Curr Opin Chem Biol 7:252-264
29. Kim GJ, Kim HS (1998) Biochem J 330:295-302
30. Jozic D, Kaiser JT, Huber R, Bode W, Maskos K (2003) J Mol Biol 332:243-256
31. Hausinger RP (2003) Nat Struct Biol 10:234-236
32. Kuchar J, Hausinger RP (2004) Chem Rev 104:509-525
33. Kuo JM, Chae MY, Raushel FM (1997) Biochemistry 36:1982-1988
34. Shim H, Raushel FM (2000) Biochemistry 39:7357-7364
35. Smith HB, Hartman FC (1991) Biochemistry 30:5172-5177
36. Gerlt JA, Babbitt PC (2001) Annu Rev Biochem 70:209-246
37. Christianson DW, Cox JD (1999) Annu Rev Biochem 68:33-57
38. Aubert SD, Li Y, Raushel FM (2004) Biochemistry 43:5707-5715
39. Porter TN, Li Y, Raushel FM (2004) Biochemistry 43:16285-16292
40. May O, Habenicht A, Mattes R, Syldatk C, Siemann M (1998) Biol Chem 379:743-747
41. Huang CY, Yang YS (2003) Biochem Biophys Res Commun 312:467-472
42. Huang DT, Thomas MA, Christopherson RI (1999) Biochemistry 38:9964-9970
43. Desmarais W, Bienvenue DL, Bzymek KP, Petsko GA, Ringe D, Holz RC (2006) J Biol Inorg Chem 11:398-408
44. Wenzel NF, Carenbauer AL, Pfiester MP, Schilling O, Meyer-Klaucke W, Makaroff CA, Crowder MW (2004) J Biol Inorg Chem 9:429-438
45. Peraro MD, Vila AJ, Carloni P (2002) J Biol Inorg Chem 7:704-712
46. Costello A, Periyannan G, Yang KW, Crowder MW, Tierney DL (2006) J Biol Inorg Chem 11:351-58

Figure Legends

Figure 1. Binuclear metal center within the active site of hydantoinase. The coordinates were obtained from 1GKP of Protein Data Bank based on *Thermus* sp. at 1.3 angstroms resolution [15]. The amino acid sequence numbers are corresponding to His-57, His-59, Lys-148, His-181, His-237 and Asp-313 of those of *Agrobacterium radiobacter* hydantoinase studied in this report. The aligned sequence are *Thermus* sp. (1GKP), *Arthrobacter aurescens* (1GKR), *Burkholderia pickettii* (1NFG), *Bacillus* sp. AR9 (1YNY), *Bacillus stearothermophilus* (1K1D), and *Agrobacterium radiobacter* hydantoinase by using MUSIC (http://genome.life.nctu.edu.tw/MUSIC/). The six conserved ligands were highlighted by black square.

Figure 2. Reactivation of apo-hydantoinase with cobalt ions. **(a)** Titration curve of hydantoinase activity with cobalt ion. The apo-hydantoinase (50 μM) was incubated with the indicated amounts of cobalt chloride in 10 mM HEPES at pH 7.0 (100 μl of final volume) for 4 days at 4 °C. The activity of hydantoinase of hydantoinase was then determined by standard assay. **(b)** Proposed kinetic model for the metal-activated hydantoinase.

Figure 3. Chemical rescue of K148A with short-chain carboxylic acids. Specific activity was determined based on standard assay. The reaction mixture included K148A, cobalt chloride (5 mM) and varying concentrations of acetic acid (open squares), propionic acid (open triangles), or butyric acid (open diamonds) and reagents needed for standard assay. The control experiment (closed circles) included varying concentrations of butyric acid in the absence of metal ion. Carboxylic acids were dissolved in assay buffer with pH adjusted. High concentration of carboxylic (>50mM) caused irreversible precipitation of K148A.

Figure 4. The pH profiles of D313E using 5-leucinyl-hydantoin as the substrate. Enzymatic activity was determined using 100 μg to 5 mg D313E. Closed circles denote k_{cat} and closed squares denote k_{cat}/K_m.

Figure 5. Mechanism of hydantoinase catalyzed reaction. (a) Resonance forms for carbamate of carboxylated lysine. (b) Resonance forms for carboxylate. (c) Proposed mechanism for the action of hydantoinase. For the hydrolysis of 5'-monosubstituted hydantoin, a nucleophilic attack by the bridging hydroxide was facilitated by the transfer of the proton from the hydroxide to the carboxylate of Asp313.

Table 1. Metal contents and specific activities of recombinant hydantoinase purified from zinc-, cobalt-, manganese-amended and unsupplemented cultures[a]

Metal ion amended (1 mM) in cell culture	Metal-amended[b] Hydantoinase (μmol/min mg)	Metal-reconstituted Hydantoinase (μmol/min mg)	Metal per enzyme subunit[c]			
			Zn	Co	Mn	Fe
Zn	0.15 ± 0.04	0.22 ± 0.03	1.4 ± 0.1	0.0 ± 0.0	0.1 ± 0.0	0.6 ± 0.3
Co	0.85 ± 0.10	1.1 ± 0.1	0.3 ± 0.1	1.2 ± 0.3	0.1 ± 0.1	0.5 ± 0.2
Mn	0.34 ± 0.05	0.45 ± 0.08	0.2 ± 0.1	0.0 ± 0.0	1.5 ± 0.2	0.3 ± 0.2
Unsupplemented	$< 10^{-4}$	-	0.3 ± 0.2	0.0 ± 0.0	0.2 ± 0.1	1.1 ± 0.3

[a] Specific activity was determined using phthalimide as substrate.

[b]Metal-amended hydantoinase was enzyme purified from metal-amended cell culture but was not gone through the procedure for metal reconstitution as described in Material and Method section.

[c] The metal contents in hydantoinase were determined by ICP-MS.

Table 2. Substrate specificity of the metal-reconstituted hydantoinase[a]

Metal ion	Substrate[b]	K_m (mM)	k_{cat} (s^{-1})	k_{cat}/K_m ($M^{-1}s^{-1}$)
Co	dihydrouracil	50 ± 20	14.0 ± 6.0	290 ± 130
	phthalimide	6.0 ± 2.0	7.7 ± 2.0	1320 ± 430
	5-leucinyl-hydantoin	4.3 ± 0.2	64 ± 1	15000 ± 700
Zn	dihydrouracil	20 ± 3	3.7 ± 1.5	190 ± 70
	phthalimide	5.3 ± 1.6	2.2 ± 0.4	420 ± 130
	5-leucinyl-hydantoin	5.3 ± 0.5	10 ± 1	1900 ± 190
Mn	dihydrouracil	80 ± 20	4.2 ± 2.0	50 ± 30
	phthalimide	8.0 ± 1.0	5.9 ± 1.4	740 ± 180
	5-leucinyl-hydantoin	5.6 ± 0.4	50 ± 4	8900 ± 700

[a]Enzymatic activity was determined according to procedure for the standard assay except that different substrates were used. The large standard errors reflected the difficulty of obtaining enzyme activity at high substrate concentrations due to the low solubility of substrates. The following compounds were judged as inactive for all the metal reconstituted hydantoinase examined: barbituric acid, dihydroorotate, uracil, pyromellitic diimide, phthalic anhydride, 5-bromouracil, 2,3-naphthalene-dicarboximide, bemegride, *N*-methyl-phthalimide, rhodanine, 1,8-naphthalimide, *N*-methylmaleimide, 4-amino-1,8-naphthalimide, 2*H*-1,3-benzoxazine-2,4(3*H*)dione, 3,4,5,6-tetrachlorophthalimide, biuret, 5,5-dimethyl-hydantoin, uridine, parabanic acid, 5-ethyl-methyl-hydantoin, oxindole, 2,4-thiazolidinedione, *N*-cyclohexylmaleimide, and *N*-hydroxyphthalimide.

[b]Structures of the three representative substrates

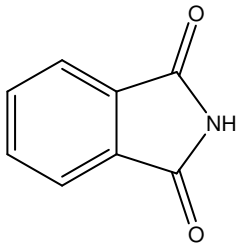

Phthalimide

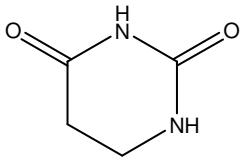

Dihydrouracil

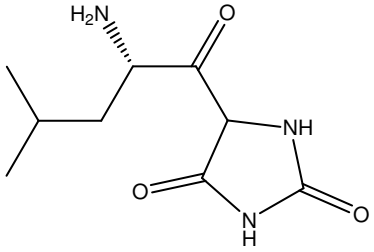

5-leucinyl-hydantoin

Table 3. The specific activity and metal content of the cobalt-reconstituted hydantoinase and mutants[a]

Enzyme	Cobalt content per enzyme subunit	Specific activity[b] (μmol/min/mg)
wild-type	2.5 ± 0.1	1.1 ± 0.1
H57A	1.2 ± 0.1	$< 10^{-4}$
H59A	1.2 ± 0.1	$< 10^{-4}$
K148A	0.5 ± 0.1	$< 10^{-4}$
K148C	0.8 ± 0.2	$< 10^{-4}$
K148D	0.8 ± 0.2	$< 10^{-4}$
K148S	0.9 ± 0.0	$< 10^{-4}$
H181A	1.2 ± 0.1	$< 10^{-4}$
H237A	1.2 ± 0.1	$< 10^{-4}$
D313A	1.4 ± 0.1	$< 10^{-4}$
D313E	2.2 ± 0.1	0.05 ± 0.01

[a]The mutant enzymes were purified from cobalt-amended cultures; the apo-hydantoinase was prepared and then reconstituted with cobalt. Prior to the performance of ICP-MS analysis, the protein solution was passed through a HiTrap™ desalting column eluted with HEPES buffer (pH 7.0, 10 mM) at 4 °C to remove excess metal ions.

[b]Assayed with phthalimide as the substrate.

Figure 1

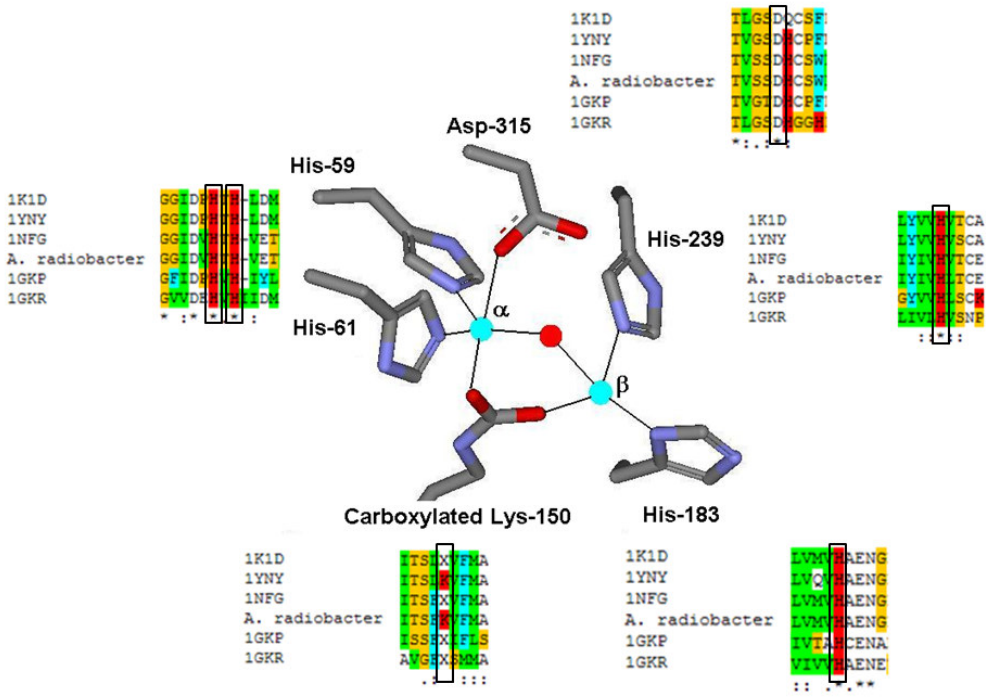
Asp-315
His-59
His-239
His-61
α
β
Carboxylated Lys-150
His-183
1K1D
1YNY
1NFG
A. radiobacter
1GKP
1GKR

Figure 2

a

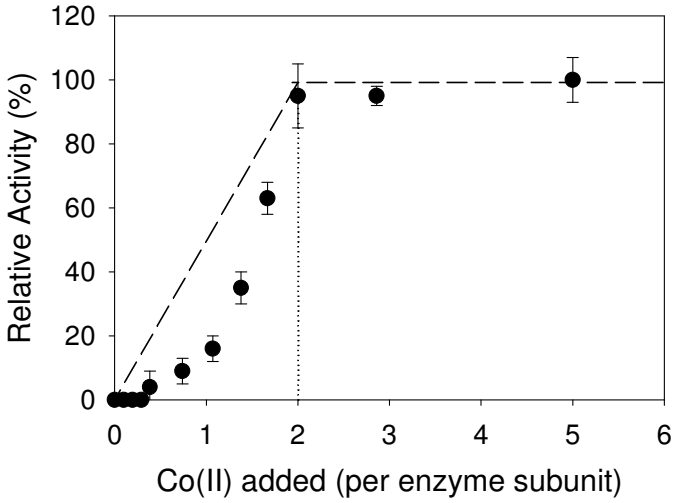
120
100
80
60
40
20
0
Relative Activity (%)
0
1
2
3
4
5
6
Co(II) added (per enzyme subunit)

b

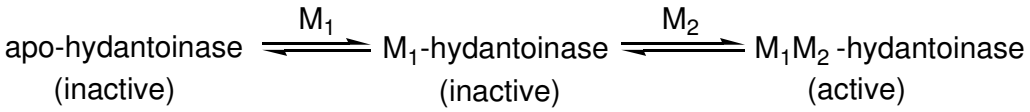
apo-hydantoinase
(inactive)
M1
M1-hydantoinase
(inactive)
M2
M1M2 -hydantoinase
(active)

Figure 3

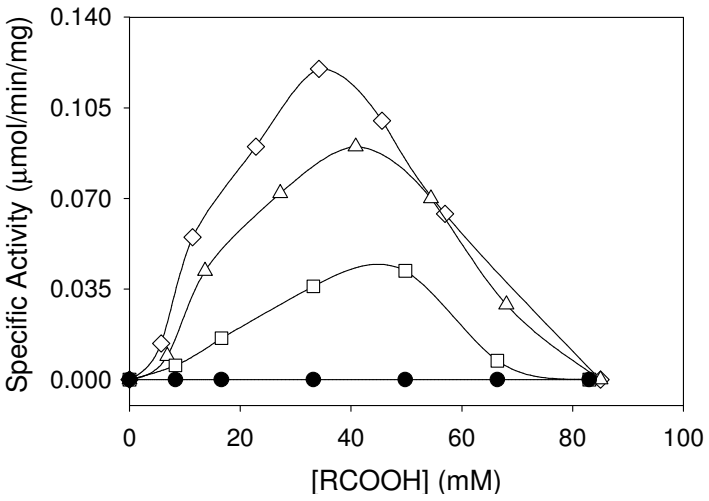
0.140
0.105
0.070
0.035
0.000
Specific Activity (µmol/min/mg)
0
20
40
60
80
100
[RCOOH] (mM)

Figure 4

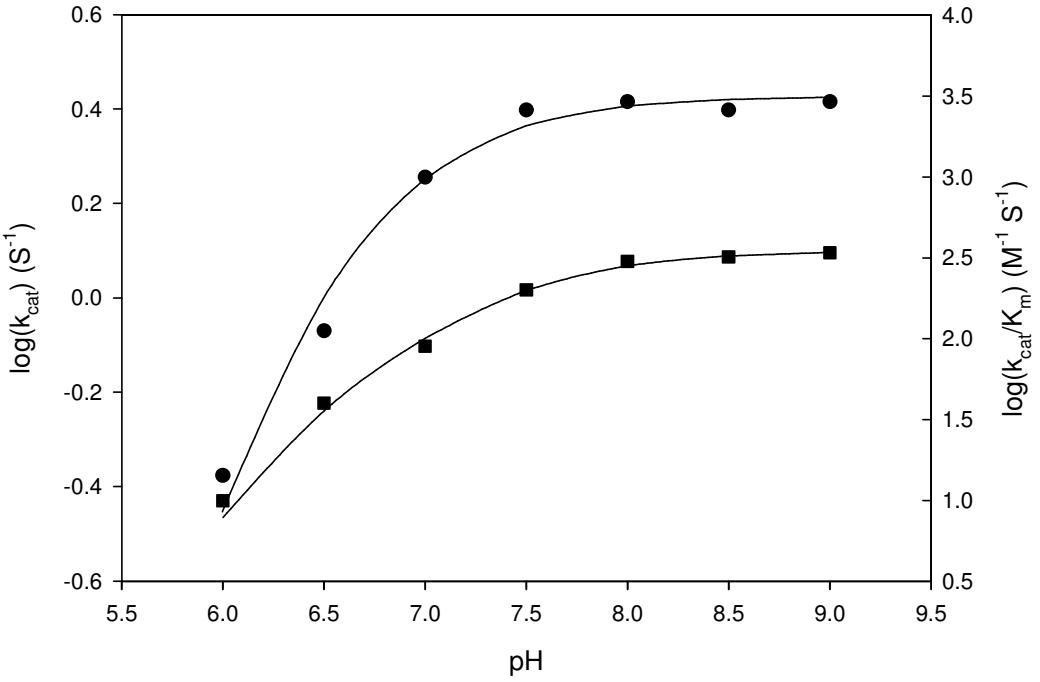
0.6
0.4
0.2
0.0
-0.2
-0.4
-0.6
4.0
3.5
3.0
2.5
2.0
1.5
1.0
0.5
5.5
6.0
6.5
7.0
7.5
8.0
8.5
9.0
9.5
pH
log(k_cat) (S^-1)
log(k_cat/K_m) (M^-1 S^-1)

Figure 5

a

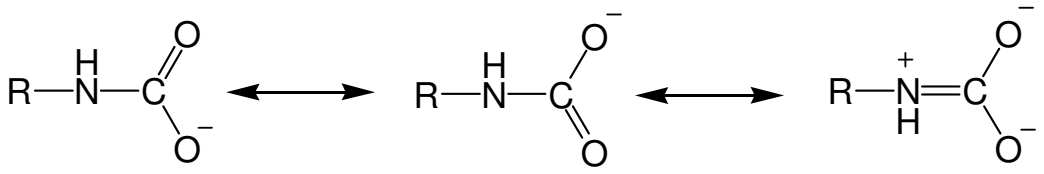

Carbamate

b

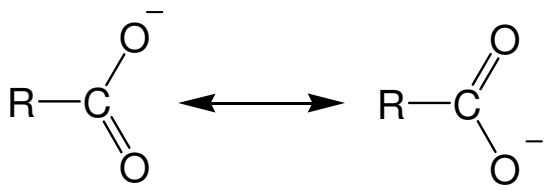

Carboxylate

c